*Journal of the Geological Society, London,* Vol. **169**, 2012, pp. 83–97. doi: 10.1144/0016-76492011-031.

# Constraints on palaeodrainage evolution induced by uplift and exhumation on the southern flank of the Zagros–Iranian Plateau

S. KHADIVI[1,2], F. MOUTHEREAU[1,2]*, J. BARBARAND[3], T. ADATTE[4] & O. LACOMBE[1,2]

[1]*UPMC Université Paris 06, UMR 7193, ISTEP, F-75005, Paris, France*

[2]*CNRS, UMR 7193, ISTEP, F-75005, Paris, France*

[3]*Université Paris Sud, UMR CNRS–UPS 8148 IDES, Bâtiment 504, Orsay cedex, F-91405, France*

[4]*IGP, University of Lausanne, Bldg Anthropole, CH-1015, Lausanne, Switzerland*

**Corresponding author (e-mail: frederic.mouthereau@upmc.fr)*

**Abstract:** Foreland sedimentary rocks from the northern Fars region of Iran contain a record of deformation associated with the Cenozoic collision between Arabia and Eurasia that resulted in formation of the Zagros orogen. The timing of the deformation associated with this event is poorly known. To address this we conducted a study of Miocene foreland sedimentary rocks (19.7–14.8 Ma) of the Chahar–Makan syncline using clast composition, clay mineralogy and low-temperature fission-track dating. The results showed that most of the sedimentary rocks were sourced from ophiolitic rocks. Detrital apatite fission-track (AFT) age signatures of Miocene sedimentary rocks record exhumation in the hanging wall of the Main Zagros Thrust and confirm that the change from underthrusting of the stretched Arabian margin to widespread crustal thickening and deformation in the Zagros region is no younger than 19.7 Ma. A transition from Late Oligocene to Mesozoic–Eocene AFT detrital age signatures between 19.7–16.6 Ma and 16.6–13.8 Ma is interpreted to reflect a possible rearrangement of palaeodrainage distribution that resulted from folding and expansion–uplift of the Zagros–Iranian Plateau region.

**Supplementary material:** Details of the succession of the study area, a complete presentation of sample preparation and fission-track age measurements of apatite grains, and examples of X-ray diffractograms are available at http://www.geolsoc.org.uk/SUP18502.

Knowledge of the distribution and timing of Cenozoic shortening as well as the magnitude of rock uplift and exhumation of the Zagros collision and the adjacent Turkish–Iranian Plateau are critical to a better understanding of how Arabian plate motion was accommodated during the collision with the overriding Eurasian plate. This is particularly important if plate reconstructions are used to infer the connectivity between the Indo-Pacific Ocean, the Mediterranean Sea and the Para-Tethyan Sea (e.g. Kocsis *et al*. 2009; Reuter *et al*. 2009), to interpret the impact of the Arabian plate–Eurasian plate convergence on the regional aridification of Central Asia (Ramstein *et al*. 1997; Gavillot *et al*. 2010; Sun *et al*. 2010) and on the Cenozoic global climate changes (Allen & Armstrong 2008), or to examine the mechanisms of Iranian Plateau uplift (e.g. Hatzfeld & Molnar 2010; Mouthereau 2011).

A wealth of new data has provided insights into the onset of the Zagros collision, which is dated to between 35 and 20 Ma (e.g. Agard *et al*. 2005; Vincent *et al*. 2005; Mouthereau *et al*. 2007*b*; Allen & Armstrong 2008; Homke *et al*. 2009; Morley *et al*. 2009; Ballato *et al*. 2011). Uncertainties in the timing of the collision have been interpreted to be related to the transition from the early 'soft' Eocene collisional stage involving the underthrusting of the stretched Arabia continental margin to the Miocene stage when the unstretched portion of the continental lithosphere started to collide with the Iranian plate (Ballato *et al*. 2011).

In this view, the Miocene stage is expected to have recorded the onset of rapid uplift, deformation and exhumation in the Zagros. The replacement of the Oligocene carbonates by the onset of coarse-grained deposition in the Zagros foreland (e.g. Fakhari *et al*. 2008), the onset of collision stress build-up and reactivation of inherited faults in the stable Arabian platform (Lacombe *et al*. 2006; Mouthereau *et al*. 2006, 2007*b*; Ahmadhadi *et al*. 2007), and Miocene apatite fission-track (AFT) and (U–Th)/He cooling ages (Gavillot *et al*. 2010; Homke *et al*. 2010) dating the earliest phase of folding in the northern Zagros Fold Belt at 14–15 Ma (Khadivi *et al*. 2010) support this timing. Such results are consistent with the observation that a marine gateway connecting the Mediterranean Sea and the Indo-Pacific Ocean existed at least until the early Miocene in Central Iran (Schuster & Wielandt 1999; Harzhauser *et al*. 2007) and until *c*. 15 Ma on the Arabian margin as indicated by *in situ* marine nannofossils of this age in the northern Zagros (Khadivi *et al*. 2010).

Surface uplift of the Zagros belt to elevations of up to 2–2.5 km has been proposed to result from a continuum of crustal thickening involving not only the Arabian margin but also the previously thinned Iranian continent (Mouthereau 2011). As collision continued, the Zagros–Iranian Plateau expanded southward into the Zagros fold belt, as seen from the development of a high elevated low-relief area (Figs 1 and 2) but the timing of these changes has not yet been defined. A study of the temporal evolution of uplift and exhumation in this northern Zagros region is therefore needed to constrain the building of the Zagros–Iranian Plateau topography. This will solve the question of whether exhumation and deformation have been synchronous along the strike of the Zagros collision and help to explain how foreland drainage patterns and exhumed source areas responded to increased tectonic forcing and formation of the Zagros–Iranian Plateau. To address these questions, we studied the provenance of Early Miocene foreland sedimentary rocks (19.7–14.8 Ma) from the northern Zagros of the Fars region.

## Geological background

The NW–SE-trending Zagros orogeny, which is part of the much larger Alpine–Himalayan orogenic system, extends some 2000 km from the East Anatolian Fault in eastern Turkey to the Makran subduction accretionary complex in southern Iran (Fig. 1). Global

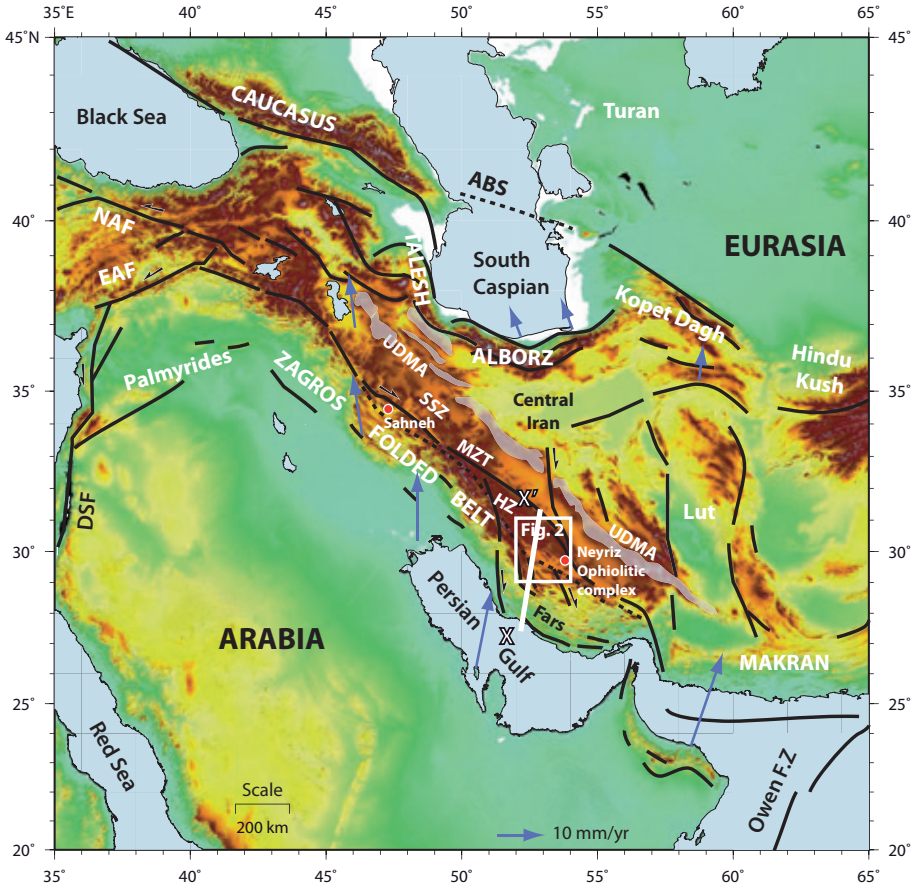


**Fig. 1.** Shaded relief and main tectonic features of the Arabia–Eurasia convergence. Bold black lines, major faults; arrows, GPS velocities from Vernant *et al*. (2004) and Masson *et al*. (2007); white circles, Sahneh (S) and Neyriz (N) ophiolitic complexes; white rectangle, location of Figure 2. SSZ, Sanandaj–Sirjan Zone; UDMA, Urumieh–Dokhtar Magmatic Arc; ABS, Apsheron–Balkan Sill; MZT, Main Zagros Thrust; HZ, High Zagros; EAF, East Anatolian Fault; NAF, North Anatolian Fault; DSF, Dead Sea Fault; F.Z, fracture zone. Grey-filled areas indicate the approximate geographical extent of the Urumieh–Dokhtar Magmatic Arc.

positioning system (GPS)-derived velocity data show present-day convergence rates between Arabia and Eurasia of 19–23 mm a$^{-1}$ (McClusky *et al*. 2003) with about a half to a third (i.e. 7–10 mm a$^{-1}$) of this accommodated by deformation within the Zagros belt (Tatar *et al*. 2002; Nilforoushan *et al*. 2003; Vernant *et al*. 2004). The collision belt comprises NW–SE-trending subparallel structural domains: the Zagros Fold Belt, the Sahneh and Neyriz ophiolitic complexes in the High Zagros that shape the Zagros suture zone, the Sanandaj–Sirjan Zone and the Tertiary Andean-type Urumieh–Dokhtar volcanic arc (Berberian & Berberian 1981; Berberian & King 1981; Berberian *et al*. 1982; Verdel *et al*. 2011).

## *Zagros Fold Belt*

The Zagros Fold Belt forms the currently active accretionary wedge of the Zagros collision. It is characterized in the Fars region by remarkably regular, long and large-wavelength NW–SE-trending concentric folds (Figs 2 and 3), built by folding of a 12 km thick sediment cover detached from the Cambrian Hormuz salt (e.g. Lacombe *et al*. 2007; Mouthereau *et al*. 2007*a*, *b*; Yamato *et al*. 2011). The Precambrian basement of the Arabia margin is also actively deforming.

The High Zagros belt is formed mainly from folded Mesozoic strata and radiolaritic series and ultramafic bodies of the Neyriz ophiolitic complex (Figs 2 and 3). It is bounded to the north by the Main Zagros Thrust, which is also called the Main Zagros Reverse Fault. This fault marks the plate boundary. The High Zagros Fault to the south is a currently inactive fault in our study area and does not show significant displacement.

The timing of shortening is not well constrained in the High Zagros owing to the lack of syntectonic stratigraphic markers. The presence of Eocene–Oligocene limestones unconformably overlying the Fold Mesozoic carbonaceous series (Fig. 2) shows that uplift and erosion were initiated in the early Cenozoic; that is, before the onset of deformation in the Zagros Fold Belt. This constraint, however, does not give insight into the last event of deformation and exhumation in the High Zagros.

## *Neyriz ophiolitic complex*

The Neyriz ophiolitic complex exposed to the east of the study area (Figs 2 and 3) is considered to be an allochthonous fragment of the western branch of Neotethyan oceanic lithosphere (Stocklin 1968; Golonka 2004). It contains a sedimentary assemblage of radiolarian cherts, turbidites, middle Jurassic oolitic, brecciated limestones, and Middle Cretaceous limestones (Ricou 1976). Mafic and felsic magmatism (e.g. gabbros, diorites and plagiogranites) formed the crustal basement of the Neyriz ophiolite, which is particularly well exposed in Tang-e Hana (Fig. 2). The mantle part of the obducted ophiolites contains peridotites, mainly harzburgites and dunites, with olivine and pyroxene that are variably serpentinized and planar chromite interlayers (Babaie *et al*. 2006). East of lake Bakhtegan, the Hajiabad mélange (Fig. 2), probably Mesozoic in age, is composed of Permian–Triassic limestones, radiolarian cherts, tuffs, basalts (pillow lavas) and greenschist to amphibolite metamorphic rocks lying above the basal detachment zone of the allochthonous ophiolite complex (Babaie *et al*. 2006; Sarkarinejad *et al*. 2009). Both the tectonic mélange and the ophiolite are thrust over the Pichakun deep-water radiolarian sediments dated to the Late Triassic to Middle Cretaceous (Ricou 1976; Robin *et al*. 2010). The Neyriz ophiolite complex was tectonically emplaced

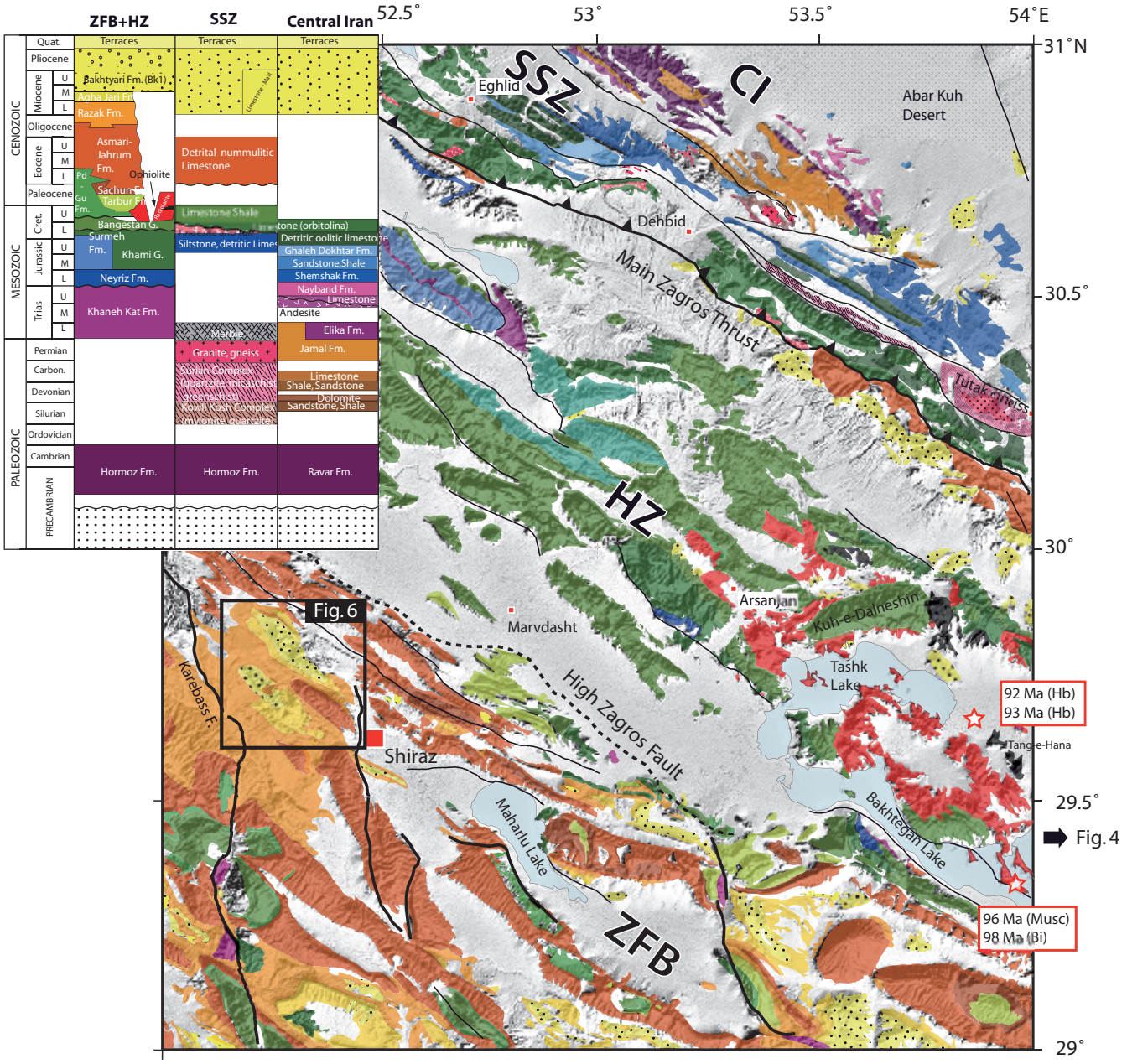


**Fig. 2.** Geological map of the Zagros (northern Fars area; location shown in Fig. 1) draped on Shuttle Radar Topography Mission (SRTM) topographic data (http://srtm.csi.cgiar.org/) and main lithostratigraphic units. The map has been mainly redrawn and simplified based on the 1/100 000 scale and 1/250 000 geological maps of Eqlid (Houshmand Zadeh *et al*. 1990) and Shiraz (NIOC 1979), respectively. The stratigraphic age of Bakhtyari Formation is from Khadivi *et al*. (2010). Red boxes show $^{40}Ar/^{39}Ar$ radiometric datings in the Neyriz ophiolitic complex after Haynes & Reynolds (1980) and Babaie *et al*. (2006). CI, Central Iran; SSZ, Sanandaj–Sirjan Zone; HZ, High Zagros; ZFB, Zagros Fold Belt. The presence of the unconformable Bakhtyari Formation in the High Zagros in the footwall of the Main Zagros Thrust should be noted.

onto the Cenomanian–Turonian shallow-marine Sarvak Formation (e.g. Hallam 1976). $^{40}Ar/^{39}Ar$ dating on hornblende in diabase and plagiogranite yielded an age of 92–93 Ma (Babaie *et al*. 2006) consistent with ages of *c*. 95 Ma obtained from amphibolites and slightly younger ages of *c*. 86 Ma from tholeiitic sheeted dykes (Lanphere & Pamic 1983). Together with the age of the unconformable limestones of the Tarbur Formation, the ophiolites have therefore been emplaced between 86 and 70 Ma (James & Wynd 1965; Hallam 1976; Ricou 1976).

### *The Sanandaj–Sirjan metamorphic belt or Sanandaj–Sirjan Zone*

The Sanandaj–Sirjan Zone to the north of the Main Zagros Thrust represents the tectonomagmatic and metamorphic part of the Zagros belt (Figs 1, 2 and 4). It comprises Palaeozoic to Cretaceous sedimentary and metamorphic rocks of the former active margin of an Iranian microcontinent that drifted during the Late Jurassic (Berberian & Berberian 1981; Golonka 2004).

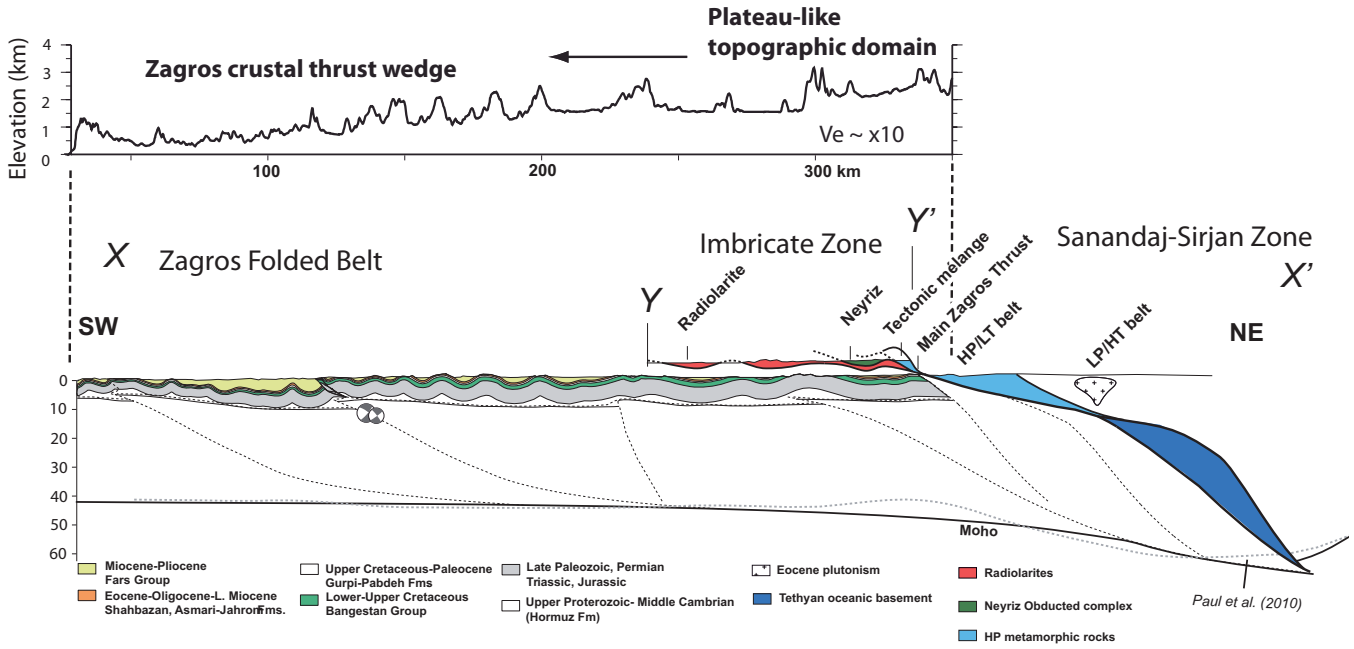


**Fig. 3.** Topographic swath profile (top) and geological section across the Zagros and the southern Iranian plateau (bottom) after a balanced cross-section proposed by Mouthereau *et al*. (2007*a*) for the Fars region (see location on Fig. 1). Section YY' is projected to show the structural position of the Neyriz obducted complex in the Imbricate Zone of northern Zagros. The boundary of the plateau-like topographic domain separates a Zagros region characterized by high elevation–low relief from the Zagros wedge topographic slope. The Moho geometry is from Paul *et al.* (2010).

From the Middle Jurassic to Early Cretaceous part of the Sanandaj–Sirjan Zone was an active margin characterized by calc-alkaline magmatic activity (Berberian & Berberian 1981). The metamorphic part of the Sanandaj–Sirjan Zone can be subdivided into HP–LT and HT–LP metamorphic belts related to a transpressional plate boundary between Iran and Arabia (Sarkarinejad & Azizi 2008). The Tutak Gneiss dome (Fig. 2) within the HP–LT belt is cored by gneisses and granites for which $^{40}Ar/^{39}Ar$ dating yielded ages of 180 and 77 Ma (Sarkarinejad & Alizadeh 2009). In the Cheh-Galatoun (Quri) metamorphic mélange (Fig. 4), east of the Neyriz obducted complex, amphibolites, garnet-bearing amphibolites and some eclogites and kyanite schists are exposed (Sarkarinejad *et al*. 2009). $^{40}Ar/^{39}Ar$ dating of the Quri amphibolites yielded an age of *c*. 91 and 112–119 Ma in biotite gneiss (Fig. 4). This cooling event is most probably related to burial and final exhumation of these rocks in an accretionary prism during the Cretaceous. The HT–LP belt to the north (Figs 2 and 3) is presumably older and related to regional metamorphism (Sarkarinejad & Azizi 2008). Magmatism resumed in the Palaeocene–Eocene when gabbroic intrusions (Gaveh-Rud pluton; see Leterrier 1985; Mazhari *et al*. 2009) or granitic intrusions of this age (Gaiduh granite) were emplaced (Rachidnejad-Omran *et al*. 2002). The Miocene emplacement of the Sanandaj–Sirjan units along the Main Zagros Thrust is revealed by the thrusting of the Cretaceous limestones over Eocene and Miocene sedimentary rocks, south of Eghlid (Fig. 2).

## *The Urumieh–Dokhtar Magmatic Arc*

The Urumieh–Dokhtar magmatic assemblage (Fig. 1) is interpreted as a subduction-related arc that has been active from the Late Jurassic to the present (Berberian & King 1981; Berberian *et al*. 1982; Verdel *et al*. 2011). Volcanism began in the Eocene and continued for the rest of that period with a climax in the Middle Eocene

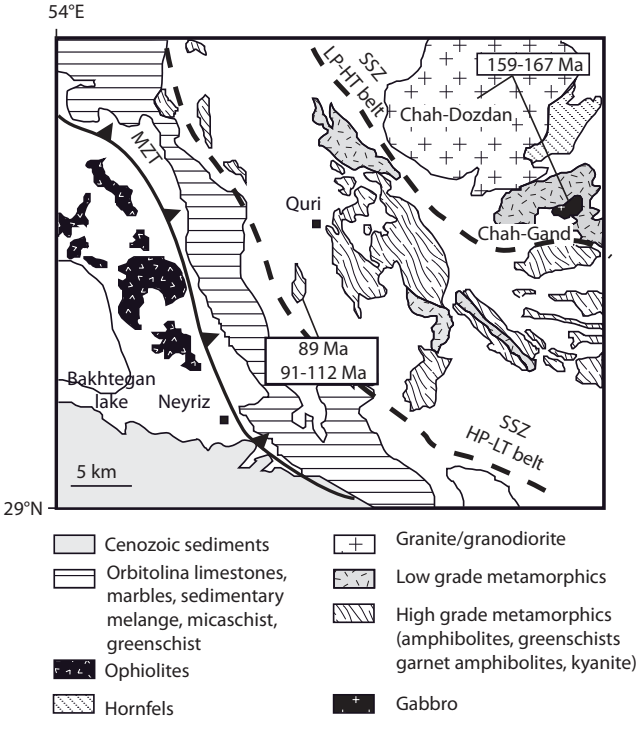


**Fig. 4.** Geological map of the northern Fars area, modified after Sheikholeslami *et al*. (2008), including the Neyriz ophiolitic complex and the low- and high-grade metamorphic belts of the Sanandaj–Sirjan Zone. $^{40}Ar/^{39}Ar$ radiometric datings of the Quri metamorphic mélange is from Haynes & Reynolds (1980) and Sarkarinejad *et al*. (2009). Ages of the Chah-Gozdan and Chah-Ghand plutonic massifs are from Sheikholeslami *et al*. (2008).

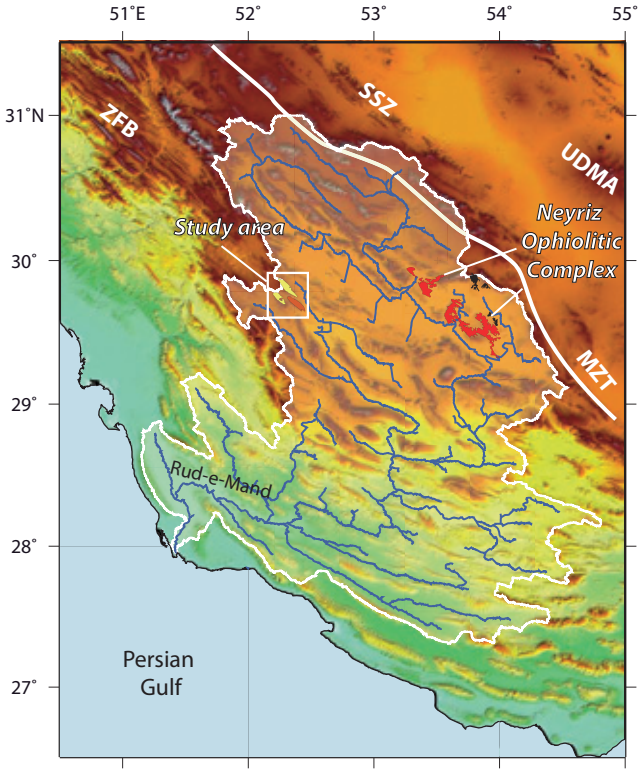


**Fig. 5.** Topographic map of the Fars area (SRTM 90 m digital elevation data; http://srtm.csi.cgiar.org/) illustrating the spatial relationships between the Rud-e-Mand river catchment and the location of the study area (see also Fig. 2). The drainage basin is characterized by the axial course of rivers running parallel to NW–SE-trending anticlines, indicating that the drainage system has been strongly controlled by fold growth. In the northern Zagros Fold Belt and High Zagros, rivers are characterized by low channel gradients and are connected to intermontane depressions occupied by salt lakes and sabkhas. The current location of the Neyriz ophiolitic complex, which is the main outcropping tectonometamorphic feature of the Fars catchment, is also displayed. The main tectonic units including the metamorphic belt of the Sanandaj–Sirjan Zone (SSZ), the Urumieh–Dokhtar Magmatic Arc (UDMA), the Zagros Fold Belt and the Main Zagros Thrust (MZT) are also shown.

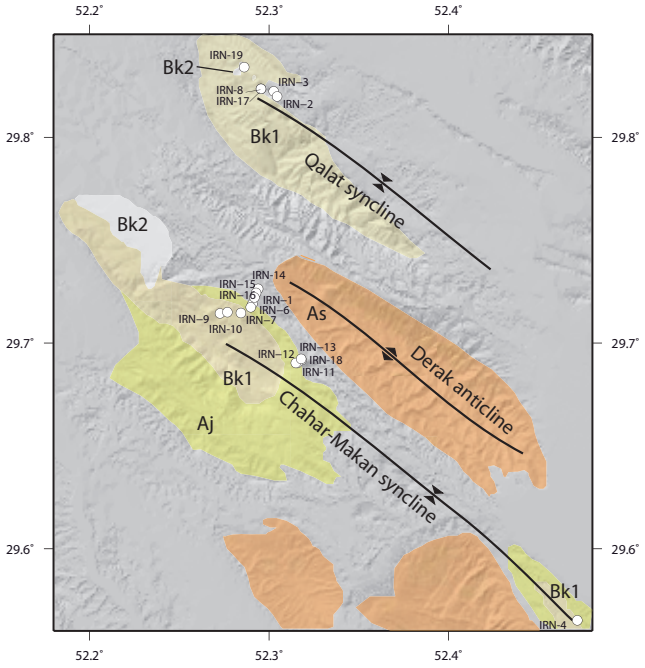


**Fig. 6.** Location of sampled sandstones for fission-track dating and petrography superimposed on a 30 km digital elevation model based on digitized topographic maps of the northern Fars domain and a simplified geological map of the study area. Aj, Agha Jari Formation; Bk1, Bakhtyari 1 Formation; Bk2, Bakhtyari 2 Formation.

(Berberian & King 1981). The oldest rocks in the Urumieh–Dokhtar Magmatic Arc are calc-alkaline magmatic rocks, which cut across Upper Jurassic formations and are overlain unconformably by Lower Cretaceous fossiliferous limestone. The youngest rocks in the Urumieh–Dokhtar Magmatic Arc consist of lava flows and pyroclastic deposits that belong to Pliocene to Quaternary volcanoes of alkaline and calc-alkaline nature (Berberian & Berberian 1981). Surface uplift of the Urumieh–Dokhtar Magmatic Arc and Central Iran to elevations of 3 and 1 km, respectively, has been recently examined through structural and basin analyses (Morley *et al*. 2009). This study suggested that short-wavelength–large-magnitude shortening, uplift and erosion took place after 10 Ma.

## Study area: main tectonic, morphological and stratigraphic features

The study region is located in SW Iran, in the Fars province (Fig. 2). It is positioned in the Mand river (Rud-e-Mand) catchment (*c*. 78 000 km$^2$), which is currently draining both the High Zagros and the Zagros Fold Belt (Fig. 5). Well-dated synorogenic deposits crop out along the northern flank of the Chahar–Makan syncline bordering the NW–SE-directed Derak anticline to the south (Figs 6 and 7).

The studied foreland succession includes, from bottom to top, the Razak, Agha Jari and Bakhtyari Formations. The Razak Formation is represented by a 500 m thick sequence of thin sandstones and yellow calcareous beds that alternate with siltstones and clays, and occasional thin gypsum beds deposited in a coastal sabkha environment. The thickness of the Agha Jari Formation is *c*. 400 m and consists of reddish marine sandstones and metre-scale conglomeratic sheets interbedded with thick (up to 20 m) intervals of red siltstones. Sandstone beds are often thicker than 2–3 m, and conglomerates include limestone cobbles of Palaeogene and Cretaceous formations of up to 10 cm (Khadivi *et al*. 2010). The presence of bidirectional current ripples as well as frequent cross-bedding laminations in sandstones points to a proximal deltaic environment. Above, the Bakhtyari 1 Formation corresponds to clast-supported, poorly sorted, and well-rounded conglomerates arranged as thick channel-like conglomeratic beds interbedded with trough cross-bedded sandstones. Clasts of the Bakhtyari 1 Formation are radiolarian cherts (<10 cm) and well-rounded pebbles of Mesozoic limestones and Nummulitic limestones of the Asmari–Jahrom Formation, with diameters up to 30 cm. Current directions show a pronounced south-directed flow, transverse to the NW-directed structures. Khadivi *et al*. (2010) interpreted these sediments as subaqueous debris flows and migrating barforms in an alluvial fan of a fluvial-dominated river delta.

## Bulk petrography, provenance and clay mineralogy of Miocene sediments

### *Sampling, experimental and analytical procedure*

To constrain sediment provenance of the Miocene foreland sedimentary rocks we studied the bulk petrography of 12 sandstone

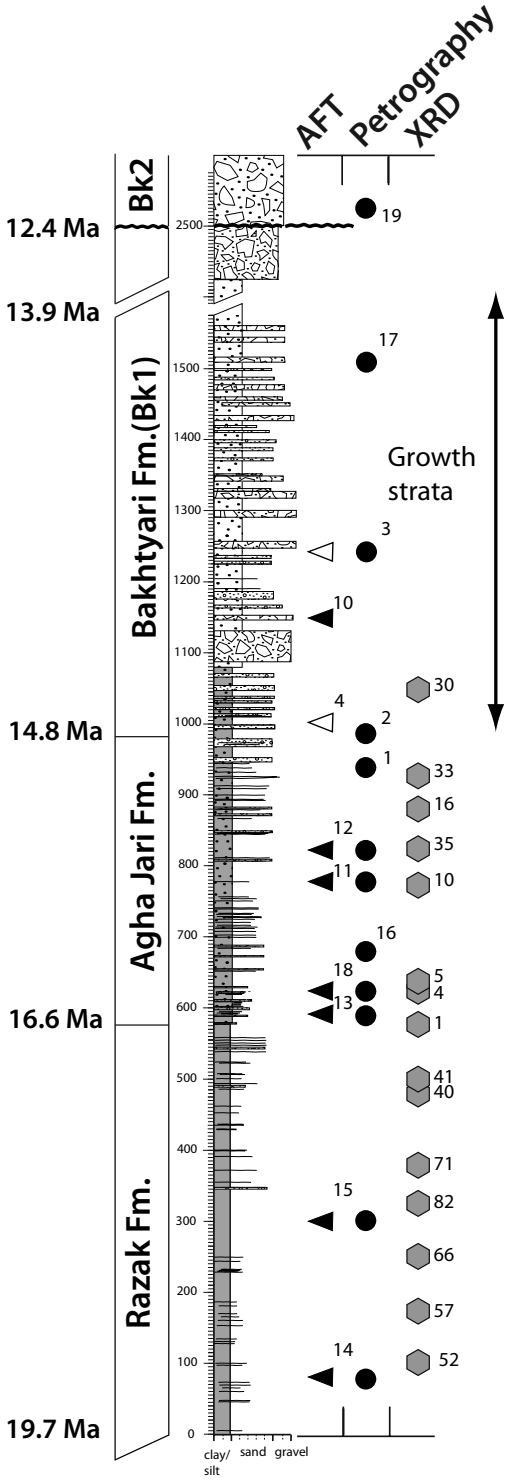


**Fig. 7.** Synthetic stratigraphic log of the Chahar–Makan syncline modified after Khadivi *et al*. (2010). The position of studied samples for petrography (black-filled circles), clay analysis (grey-filled hexagons) and fission-track thermochronology (IRN samples mentioned in the text) is also shown as black and white triangles for in-section and projected samples (see Fig. 6 for location), respectively. Grain sizes are indicated at the base of the stratigraphic column (subdivisions in sands are for very fine, fine, medium, coarse and very coarse, and in gravels for pebble and cobble sizes). Bk1, Bakhtyari 1 Formation; Bk2, Bakhtyari 2 Formation. The age of 12.4 Ma for the base of Bk2 conglomerates is derived from extrapolation of accumulation rate obtained in Bk1.

samples (Fig. 7 and Table 1) collected in fine- to medium-grained sandstones from the Razak (two samples), Agha Jari (seven samples) and Bakhtyari 1 (two samples) Formations (Figs 6 and 7) and along the Chahar–Makan sections. The last were also subjected to AFT analysis. Above the major unconformity between Bk1 and Bk2 we collected one additional sandstone cobble.

Thin sections study of the 12 sandstones included mineral assessment using the Gazzi–Dickinson method (e.g. Ingersoll *et al*. 1984) based on 300 point counts per thin section. Each sandstone was analysed by SEM and 15 samples collected in silty intervals were analysed by X-ray diffraction (XRD) to capture the full mineral compositional range. SEM images were obtained on unpolished carbon-coated thin sections analysed using a Philips XL 30 SEM (IDES, University Paris-Sud).

Bulk-rock and clay mineral assemblages were performed by XRD (ARL X'TRA Diffractometer) based on procedures described by Kübler (1983) and Adatte *et al*. (1996). The semi-quantification of whole-rock mineralogy is based on XRD patterns of random powder samples by using external standards with a margin of error between 5 and 10% for the phyllosilicates and 5% for grain minerals.

Clay mineral analysis followed methods developed by Kübler (1987) and Adatte *et al*. (1996). The abundances of the identified minerals were measured for a semi-quantitative estimate of the proportion of clay minerals, which is given as relative per cent without correction factors, because of the small margin of error (<5%). When necessary, identification of palygorskite main reflections (8.4–8.9 2Θ) have been obtained by deconvolution using a Pearson type 7 function.

### *Detrital petrological composition of Miocene sediments*

To try to discriminate sandstone provenance a spectrum of key indices is calculated on different classes of lithic grains (Ingersoll *et al*. 1984; Fig. 8 and Table 1).

A QtFL (total Quartz–Feldspar–Lithic grains) ternary diagram (inset of Fig. 8) presents the petrological composition of the various stratigraphic levels (Razak, Agha Jari and Bakhtyari Formations) and shows that all originated from recycled lithic grains of an eroded arc–orogen system. In detail, the QpLvmLsm plot (polycrystalline quartz–volcanic and volcano-metamorphic lithic grains–sediment and metamorphic lithic grains) emphasizes that the petrographic pattern of detrital minerals from bottom to top is dominated by volcanic grains and sediment lithic grains in proportions varying between 20 and 70% (Fig. 8). Sedimentary lithic grains are almost exclusively composed of red cherts, chiefly radiolarian in origin, and bioclasts. Scanning electron microscopy shows volcanic minerals including olivine, pyroxene and plagioclase. The association with accessory heavy minerals such as garnet, kyanite, rutile, chromite, titanite and ilmenite points toward an ultramafic source.

Statistical analysis of the QpLvmLsm ternary plot shows a shift with time in mean composition towards sedimentary lithic grains (Fig. 8 and Table 1). At the base of the foreland series the volcanic lithic grains component is dominant (60–80%). Up section, the relative proportion of sediment lithic grains increases to attain about 70% in the Bk1 conglomerates.

The XRD bulk-rock composition (Fig. 9a) obtained from 15 shaly and silty intervals (Fig. 6) exhibits three main components: calcite (*c*. 40%), phyllosilicate (>20%) and quartz (including chert) (*c*. 20%). Dolomite (10%) and ankerite (Fe-rich dolomite) (10%) are also important components, with minor feldspar (plagioclase and K-feldspar). Together with the presence of detrital serpentines,

**Table 1.** *Calculated sandstone point-count data (Gazzi–Dickinson method)*

| Sample | Formation | Qt | F | L | Qp | Lvm | Lsm | Lv | Lc | Lch | Lm |
|---|---|---|---|---|---|---|---|---|---|---|---|
| IRN 19 | Bk2 | 10.9 | 0 | 89.1 | 9.5 | 20.1 | 70.4 | 31.6 | 54.3 | 5.5 | 0.3 |
| IRN 17 | Bk2 | 17.9 | 0 | 82.1 | 12.9 | 13.6 | 73.5 | 13.7 | 58.8 | 14.5 | 0.0 |
| IRN 3 | Bk1 | 5 | 0 | 95 | 4.7 | 60.4 | 34.9 | 60.4 | 17 | 17 | 0.8 |
| IRN 2 | Agha Jari | 2 | 0 | 98 | 2 | 40.5 | 57.5 | 40.5 | 13.4 | 43.3 | 0.8 |
| IRN 1 | Agha Jari | 4.5 | 0 | 95.5 | 3.6 | 34.1 | 62.3 | 34.1 | 24.9 | 36.9 | 0.5 |
| IRN 12 | Agha Jari | 5.4 | 0.2 | 94.4 | 5.2 | 44.2 | 50.6 | 44.2 | 19.6 | 30.8 | 0.2 |
| IRN 11 | Agha Jari | 11.4 | 0.9 | 87.7 | 11.5 | 64 | 24.5 | 64.1 | 14.5 | 9 | 0.9 |
| IRN 16 | Agha Jari | 5.8 | 0.5 | 93.7 | 5.9 | 53.3 | 40.8 | 53.3 | 2.7 | 37.2 | 1.0 |
| IRN 18 | Agha Jari | 12.4 | 0.5 | 87.1 | 10 | 21.4 | 68.5 | 21.4 | 38.5 | 26.3 | 3.7 |
| IRN 13 | Agha Jari | 4.6 | 0.2 | 95.2 | 4.6 | 45.6 | 49.8 | 45.6 | 16.2 | 32.8 | 0.8 |
| IRN 15 | Razak | 8.5 | 2.3 | 89.2 | 7.6 | 70.9 | 21.5 | 71.7 | 4.6 | 13.3 | 2.7 |
| IRN 14 | Razak | 12.3 | 0 | 87.7 | 10.9 | 57.1 | 32.1 | 55.2 | 29.2 | 5.5 | 1.1 |

Ten primary proportional parameters and secondary ratio parameters, representing an extension of those originally proposed by Dickinson (1970), provide a synthesis of framework composition: Qt, total quartz; F, feldspars; L, total aphanite lithic grains; Qp, fine- to coarse-grained polycrystalline quartz (excluding chert); Lvm, volcanic and volcano-metamorphic lithic grains; Lsm, sedimentary and metamorphic lithic grains; Lv, volcanic lithic grains; Lc, carbonate lithic grains; Lch, chert lithic grains; Lm, metamorphic lithic grains. Lsm is the sum of Lc–Lch–Lm parameters rescaled for the QtLvmLsm ternary plot of Figure 8. No volcano-metamorphic grains have been detected so the Lvm parameter is equal to Lv.

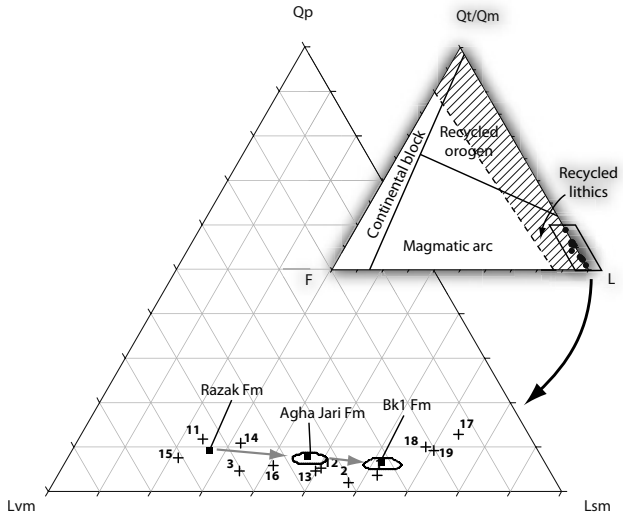


**Fig. 8.** Petrographic modes shown in Qt/QmFL and QpLvmLsm ternary diagrams for sandstones collected along the Chahar–Makan section (see Fig. 7 for stratigraphic location). Qt/QmFL diagram shows that all samples belong to recycled lithic grains from a mixed orogen and magmatic source. The calculation of the mean petrographic composition in QpLvmLsm plot for the three studied group samples of the Razak, Agha Jari and Bakhtyari 1 formations reveals the increasing amount of sediment lithic fragments up section. For the group samples the mean is shown by a black square and the 95% confidence interval by a bold black line. These quantities have been computed using the CoDaPack3D Excel-based software (http://ima.udg.edu/~thio/).

the bulk-rock composition in the record indicates weathering of ultramafic rocks with high Fe–Mg content similar to the Neyriz Obducted Complex.

### *Clay mineral assemblages*

Clay minerals are byproducts resulting from the interplay between climate, continental morphology, tectonic activity and sea-level variations, and therefore can be used as environmental proxies (Chamley 1989; Weaver 1989). Among the major clay minerals encountered in sedimentary records are kaolinite, smectite, chlorite and illite. In equatorial zones, kaolinite forms in soil under constant humid conditions as a result of high chemical weathering. Smectite originates either from tropical soil under semi-arid and seasonal climate conditions or as a weathering byproduct of basalt (Chamley 1989; Chamley *et al*. 1990; Deconinck & Chamley 1995). Chlorite–smectite mixed layers (CS) are a weathering product of Mg-enriched rocks such as basalts or serpentinites but form under more temperate and humid conditions than smectite (Chamley 1989). Illite and chlorite are byproducts of tectonic uplift and physical weathering (Chamley 1989; Robert & Chamley 1990).

The clay fraction is composed of palygorskite, smectite, chlorite and irregular to regular (corrensite type) mixed-layer chlorite–smectite and mica (Fig. 9b). The kaolinite is nearly absent from the clay assemblage. The stratigraphic column can be separated in two parts, as follows.

(1) The lower part (0–400 m, upper part of the Razak Formation) is characterized by the lack of palygorskite and the noticeable abundance of smectite, chlorite, mixed-layer chlorite–smectite and especially micas, episodically representing more than 60% of the clay fraction.

(2) The upper levels represented by Agha Jari and Bakhtyari 1 Formation are dominated by palygorskite, mixed-layer chlorite–smectite, chlorite and smectite to the detriment of mica.

## Detrital apatite fission-track thermochronology

### *Experimental and analytical procedure*

Nine samples were collected for apatite fission-track analysis along a *c*. 1600 m section in and above the dated section of the Chahar–Makan syncline (Fig. 7 and Table 2). The sampling interval is expected to be small enough to capture potential changes in the source areas.

Sample investigation including mineral separation, counting and analysis were performed in the IDES laboratory (Université Paris-Sud). Apatite grains were separated from crushed rocks using classical sieving, density and magnetic separation techniques.

### *Results*

Our samples yielded very few apatite crystals and no confined FT lengths could be measured in the nine dated samples. The AFT results from are provided in Table 2 and shown as radial plots and probability density plots (Fig. 10).

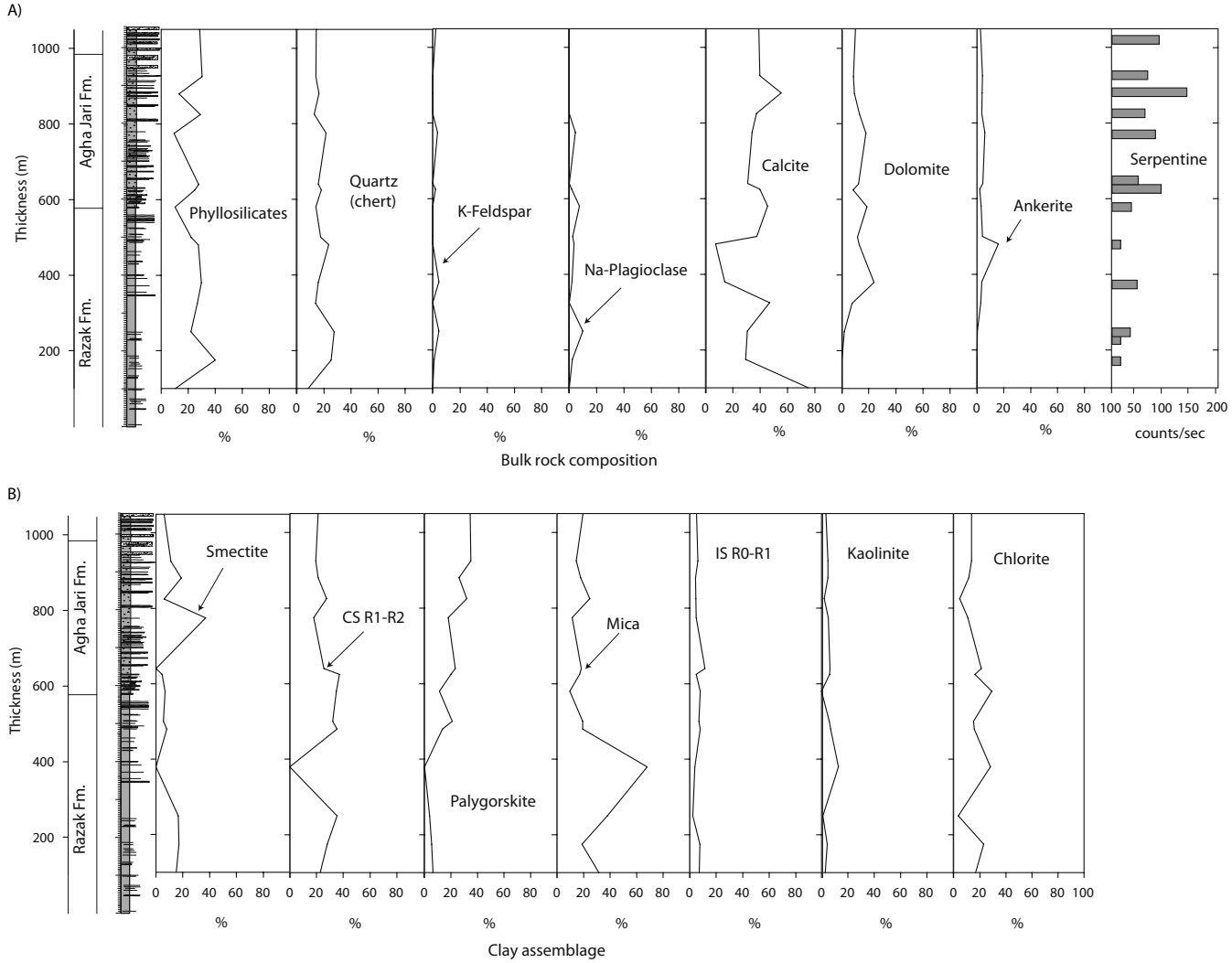


**Fig. 9.** (**a**) X-ray diffraction bulk-rock composition along the Chahar–Makan section (see location of samples on Fig. 7). Because serpentine is present as a trace in our samples the serpentine group is plotted as counts $s^{-1}$ not percentage. (**b**) X-ray diffraction clay mineral assemblages along the Chahar–Makan section.

**Table 2.** *Apatite fission-track analytical data*

| Sample | Formation | Approx. depositional age (Ma) | Depth (m) | No. of grains | $\rho_s$ ($N_s$) × $10^6$ ($cm^{-2}$) | $\rho_i$ ($N_i$) × $10^6$ ($cm^{-2}$) | $\rho_d$ ($N_d$) × $10^5$ ($cm^{-2}$) | $P$ ($\chi^2$) (%) | Disp. (%) | Central age ±2σ (Ma) | No. of $D_{par}$ | Mean $D_{par}$ (μm) | SD (μm) |
|---|---|---|---|---|---|---|---|---|---|---|---|---|---|
| IRN 3 | Bk1 | 14.2 | – | 8 | 0.16(59) | 0.90(65) | 5.141(7170) | 6.17 | 47 | 76±20 | 39 | 2.02 | 0.47 |
| IRN 10 | Bk1 | 14.3 | 1150 | 7 | 0.22(25) | 0.63(63) | 6.238(12514) | 34.9 | 23.9 | 44±12 | 45 | 1.59 | 0.23 |
| IRN 4 | Bk1 | 14 | – | 3 | 0.18(9) | 0.24(12) | 5.141(7170) | 27.7 | 11.2 | 64±29 | 13 | 1.9 | 0.27 |
| Combined (IRN 3, 10, 4) | | | | 18 | | | | 12.6 | 50 | 77±20 | | | |
| IRN 12 | Agha Jari | 15.5 | 840 | 8 | 0.09(15) | 0.25(41) | 6.371(12514) | 65.8 | 0.3 | 39±12 | – | 1.44 | 0.25 |
| IRN 11 | Agha Jari | 16 | 790 | 7 | 0.22(29) | 0.34(46) | 6.295(12514) | 89.5 | 0.1 | 66±16 | 39 | 1.88 | 0.86 |
| IRN 13 | Agha Jari | 16.4 | 620 | 7 | 0.24(31) | 0.55(70) | 6.314(12514) | 63.9 | 0.2 | 46±10 | 40 | 1.82 | 0.36 |
| IRN 18 | Agha Jari | 16.5 | 600 | 14 | 0.48(130) | 0.68(181) | 6.276(12514) | 8.94 | 28 | 72±11 | 54 | 1.78 | 0.51 |
| IRN 15 | Razak | 18 | 300 | 12 | 0.24(27) | 1.02(115) | 6.352(12514) | 77.7 | 1.4 | 25±5 | 22 | 1.03 | 0.15 |
| IRN 14 | Razak | 19.3 | 80 | 8 | 0.54(34) | 2.31(146) | 6.333(12514) | 46 | 0.02 | 24±5 | 20 | 1.14 | 0.19 |

$\rho_s$ and $N_s$, density and number of spontaneous fission tracks, respectively; $\rho_i$ and $N_i$, density and number of induced fission tracks; $\rho_d$ and $N_d$, density and number of measured in fluence dosimeter. ζ calibration factor has been determined by using the following age standards; Durango (31.4±0.8 Ma), Fish Canyon Tuff (27.9±0.7 Ma) and CN5 with 12.19 ppm U. $P$ ($\chi^2$), chi-squared probability that grain ages are concordant. Disp., age dispersion. A sample may contain multiple age populations if $P$ ($\chi^2$) <5 and/or Disp. >15 (Galbraith & Green 1990; Galbraith & Laslett 1993). SD, standard deviation of mean $D_{par}$ (μm). 'Combined' indicates the decomposition of combined grain-age distribution that was performed to obtain better resolution on dominant grain-age populations.

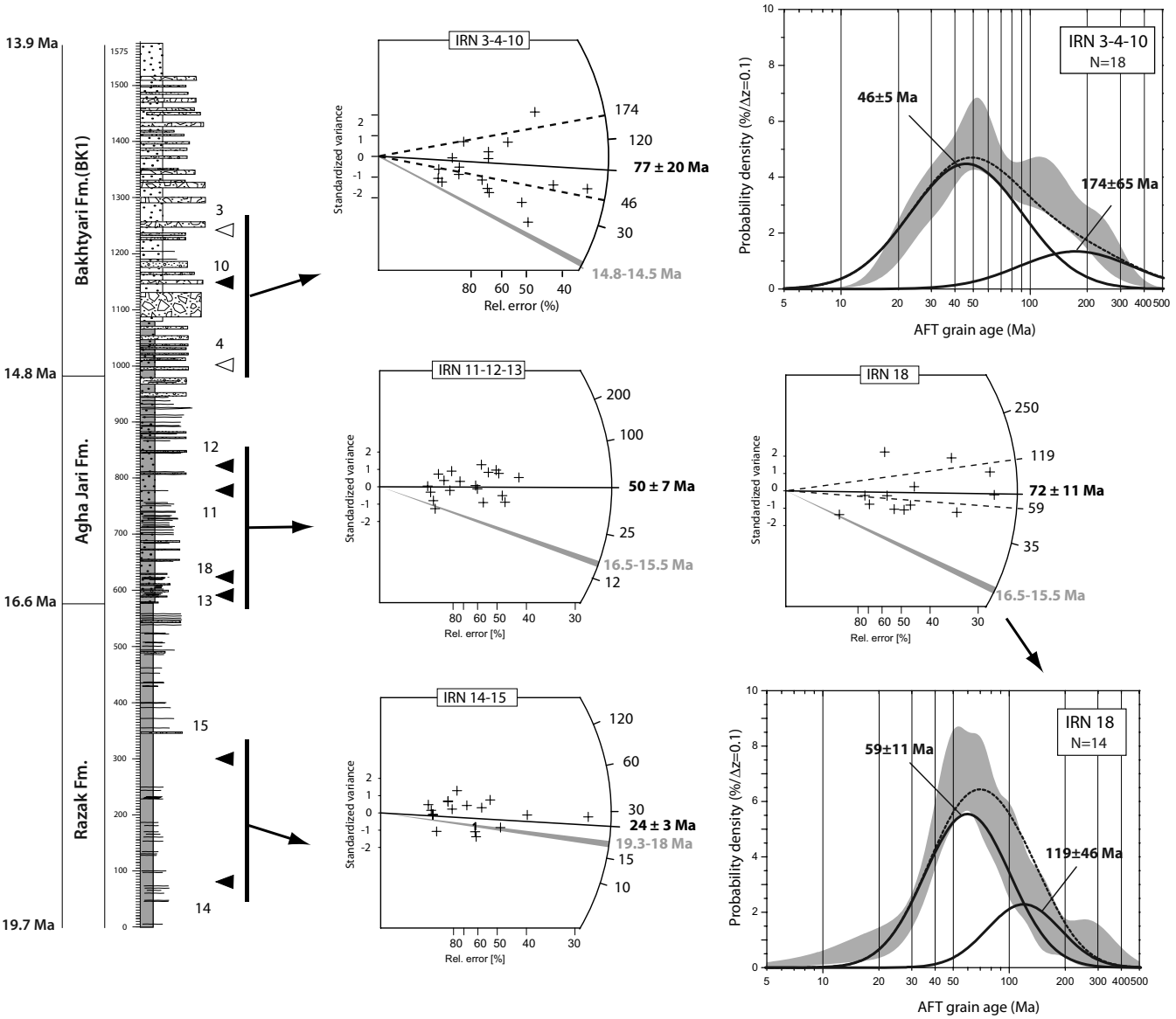


**Fig. 10.** Synthetic stratigraphic section studied along the Chahar–Makan syncline. Ages of the formations are based on Khadivi *et al*. (2010). Black triangles, apatite fission-track samples collected in the section; white triangles, samples collected nearby (see Fig. 6 for location) in the same formation. Radial plots show central ages in bold and the range of depositional age presented as grey-filled segments. Grain-age probability density plots show binomial fitted peaks of the three combined apatite populations.

Razak Formation. Sandstones from the Razak Formation contain clasts of red radiolarian cherts and ultramafic rocks that were probably derived from sources equivalent to rocks currently exposed in the Neyriz ophiolitic complex. Two samples, IRN 14 and 15, from sandstone layers located at levels 80 and 300 m of the Chahar–Makan section (Fig. 7), yielded central ages of 24 ± 5 Ma and 25 ± 5 Ma, with similar low dispersion (1.4–0.02%) and relatively high probability (46% and 77%, respectively) indicating that both samples contain single grain-age populations. A mean low $D_{par}$ value of *c*. 1 μm in both samples argues for a similar chemical composition of apatite crystals, consistent with the same sediment provenance.

Agha Jari Formation. Samples IRN 11, 12, 13 and 18 were collected in the Agha Jari Formation between levels 600 and 840 m (Fig. 7). Central ages, from bottom to top, are 46 ± 10 Ma (IRN13), 66 ±16 (IRN11) and 39 ± 12 Ma (IRN12). The component single-grain ages show a low dispersion of 0.3% (sample IRN12) consistent with a single-grain age population. Because the central ages overlap within error, the data were grouped together to define a central age of 50 ± 7 Ma as indicated on a radial plot (Fig. 10). In contrast, sample IRN18 shows a slightly higher dispersion of 28% and suggests a mixed AFT age population. Mean $D_{par}$ values between 1.4 and 1.8 μm also suggest a different provenance.

Bakhtyari 1 Formation. Samples IRN 4 and IRN 10 were collected near the top of the Chahar–Makan magnetostratigraphic section at *c*. 1150 m (Fig. 7) and correspond to sandstones found in the Bakhtyari 1 Formation. Sample IRN 3 was collected in the Qalat syncline. Its position in the Qalat section allows correlation

with the Bakhtyari 1 Formation of the Chahar–Makan section situated *c*. 5 km to the south (Fig. 6). The large age dispersion between 23 and 47% indicates mixed grain-age populations but because of the low number of dated apatites, these grain-age populations are not well constrained. Decomposition of the combined grain-age datasets (18 grains) was therefore performed to obtain better resolution of grain-age populations. We identify one dominant population with peak age of 46 ± 5 Ma and a minor population with peak age of 174 ± 65 Ma (Fig. 1). As with sample IRN 18 for the previous formation, the significance of the older population can be questioned because of the large uncertainty. Overall these results are consistent with the Eocene and Mesozoic AFT ages obtained from the Agha Jari Formation and suggest that source rocks shared a similar cooling history.

### *Constraints on Miocene cooling*

The upper levels of the studied section comprising the Agha Jari and Bakhtyari 1 Formations yielded AFT ages distinctively older than the sample rock depositional ages. This suggests that these apatite grains were not partially reset during burial in the foreland basin and therefore record source-area cooling histories.

Extrapolation of foreland sediment thickness below the Bk2 erosional surface indicates that the base of the section that corresponds to the Razak Formation was originally buried to a depth of *c*. 2.5 km (Fig. 7), which is sufficient to cause partial resetting of apatite, depending on apatite grain composition and palaeogeothermal gradient. Taking into account recent thermochronometric studies (Gavillot *et al*. 2010; Homke *et al*. 2010) and results from tectonic modelling (Mouthereau *et al*. 2006), the geothermal gradient for the region was probably in the range 15–24 °C km$^{-1}$. Given this value and assuming a surface temperature of 0 °C or 20 °C, the maximum burial temperature experienced by samples IRN 14 and 15 should be lower than *c*. 59 °C. Other lines of evidence indicating that the AFT age of *c*. 25 Ma could represent the record of a hinterland denudation include a single grain-age population older than the depositional age of 19.7 Ma at the base of the Razak Formation.

We therefore interpret the distinctive Mesozoic, Eocene and Miocene AFT ages as indicating true hinterland cooling ages. In summary, three AFT grain-age populations have been recovered from the Razak, Agha Jari and Bakhtyari 1 Formations: (1) Jurassic–Early Cretaceous (174–119 Ma); (2) Palaeocene–Eocene (66–39 Ma); (3) Late Oligocene (*c*. 25 Ma).

## Discussion

### *AFT cooling events*

*Jurassic to Early Cretaceous AFT ages: mixed Sanandaj–Sirjan Zone and tectonic mélange source areas?* The oldest AFT grain-age populations of 174 ± 65 Ma and 101 ± 46 Ma reported in the Agha Jari and Bakhtyari 1 Formations are not well represented in our samples and are therefore difficult to interpret. However, Mesozoic arc magmatism and exhumation are documented, north of the suture zone, in the southern Sanandaj–Sirjan Zone and the Quri tectonic mélange by higher-temperature thermochronometers (Ar/Ar, K/Ar; Table 3) suggesting that these AFT ages might be related to the same Mesozoic thermal and exhumational event (Figs 2 and 4).

Andesitic intrusions and gabbroic–granitic plutons in the southern Sanandaj–Sirjan Zone, SW of Shahr-e-Babak ophiolitic complex (Berberian & Berberian 1981) have yielded ages of 118 and 164 Ma from K/Ar dating of muscovite and biotite, respectively. Metamorphism in Markran amphibolite of southern Sanandaj–Sirjan Zone has been consistently dated to *c*. 170 Ma by $^{40}Ar/^{39}Ar$ on hornblende (Haynes & Reynolds 1980). Amphibolitic foliations in the Muteh metamorphic complex of the Golpaygan region in the NW of Sanandaj–Sirjan Zone have also yielded an age of *c*. 170 Ma by $^{40}K/^{40}Ar$ geochronology (Rachidnejad-Omran *et al*. 2002). Closer to our study area, the emplacement of the Chah-Dozdan granodiorite and Chah-Ghand gabbro of the Sanandaj–Sirjan magmatic arc intruded into Triassic basalts and tuffs, which is currently thrust onto the Neyriz ophiolitic complex, can be dated to the middle Jurassic (159–167 Ma) according to recent $^{40}K/^{40}Ar$ radiometric dating (Sheikholeslami *et al*. 2008). The occurrence of metamorphic pebbles within the Late Jurassic clastic sediments south of the Chah-Dozdan granodiorite shows erosion of the Jurassic accretionary prism (Sheikholeslami *et al*. 2008). Regional exhumation in the Jurassic ended with the deposition of Berriasian–Valanginian Orbitolina limestone *c*. 140 Ma (Ricou 1976; Berberian & King 1981).

Berberian & Berberian (1981) also documented many late Cretaceous intrusive bodies in the NW of the Sanandaj–Sirjan Zone (e.g Alvand, Borudjerd, Arak and Malayer plutons). The Neyriz tectonic mélange could have also been a major source for these Mesozoic AFT cooling ages. $^{40}Ar/^{39}Ar$ dating on hornblende in plagiogranite and dolerite of the Neyriz Ophiolitic complex yielded a cooling age of 92–93 Ma (Babaie *et al*. 2006). The late Campanian–Maastrichtian (*c*. 70 Ma) age of the Tarbur limestones, which unconformably overlie the ophiolites, provides constraints on the timing of obduction (James & Wynd 1965; Ricou 1976). Overall, the Mesozoic AFT age signatures recovered from the Miocene foreland sediments are consistent with cooling events reported in the HP belt to the south of the Sanandaj–Sirjan belt and the tectonic mélange and in the obducted ophiolitic complex. Accessory minerals such as garnet, amphibole and kyanite also support the erosion of the metamorphic belt.

*Early Eocene cooling–denudational event: a magmatic and exhumational event in the Sanandaj–Sirjan Zone?* Following the obduction in the late Cretaceous in the High Zagros and magmatism in the Sanandaj–Sirjan belt during the Mesozoic, calc-alkaline arc magmatism resumed in the Eocene and then shifted northwards to the Urumieh–Dokhtar Arc and the Alborz mountains (Berberian & Berberian 1981; Berberian & King 1981). The tectonic setting of this Eocene volcanic event is still debated but there is increasing evidence that it was related to post-Cretaceous extension associated with the development of metamorphic-core complexes on the Iranian plate (Verdel *et al*. 2007). Back-arc extension at *c*. 40 Ma proposed to explain both Eocene magmatism and rapid subsidence in the Talysh mountains of the South Caspian basin (Vincent *et al*. 2005) would fit with the AFT data from the Agha Jari and Bakhtyari 1 Formations, which yielded cooling ages between 66 ± 16 and 39 ± 12 Ma.

In addition to the Eocene magmatic event there are further indications of a coeval erosional event in the High Zagros. This is recorded, in the Lurestan area, by an unconformity between the *c*. 56 Ma Kashkan conglomerates sourced by the Sahneh ophiolitic suites (James & Wynd 1965; Homke *et al*. 2009) and the Shahbazan limestones dated to about 34 Ma (Homke *et al*. 2009), suggesting that erosion or non-deposition occurred in the High Zagros before subsidence in the foreland basin was initiated. During the middle to late Eocene, in the Fars area, the transition from Sachun Formation (Palaeocene–Eocene) to Jahrom dolomites (Late Eocene) at approximately the same time also documents an increase in subsidence in the Zagros Basin (Motiei 1993). The occurrence of renewed subsidence and erosion generally agrees

**Table 3.** *Summary of in situ K/Ar and Ar/Ar ages obtained for lithologies in the Sanandaj–Sirjan Zone (SSZ), the Quri tectonic mélange (see also Fig. 3) and the Neyriz obducted complex to the north or NE of the study area*

| Location | Lithology | Dating method | | Reference |
|---|---|---|---|---|
| | | K/Ar | Ar/Ar | |
| Southern SSZ | Gabbro–granite | 164 Ma (Bi)<br>118 Ma (Mu) | | 1 |
| Southern SSZ | Amphibolite | | 170 Ma (Hb) | 2 |
| NW SSZ | Amphibolite | 170 Ma (Hb) | | 3 |
| Southern SSZ | Gabbro–granodiorite | 159–167 Ma (Bi + Mu) | | 4 |
| Tectonic mélange | Metamorphic pebble | | 98 Ma (Bi)<br>96 Ma (Mu) | 2 |
| Tectonic mélange | Biotite schist | | 89 Ma (Bi) | 2 |
| Neyriz ophiolites | Plagiogranite–diabase | | 92–93 Ma (Hb) | 5 |
| Neyriz ophiolite | Amphibolite | | 95 Ma (Hb) | 6 |
| Neyriz ophiolite | Diabase | | 86 Ma (Hb) | 6 |

The mineral phase used for dating is indicated: Bi, biotite; Mu, muscovite; Hb, hornblende. References: (1) Berberian & Berberian (1981); (2) Haynes & Reynolds (1980); (3) Rachidnejad-Omran *et al*. (2002); (4) Sheikholeslami *et al*. (2008); (5) Babaie *et al*. (2006); (6) Lanphere & Pamic (1983).

with the regional occurrence of Eocene turbiditic basins in the northern Zagros (e.g. Hempton 1987). Both magmatism and exhumation observed in the High Zagros and Sanandaj–Sirjan Zone can therefore be sources for the Eocene AFT ages (Fig. 10). This complements previously published AFT ages of 39–45 Ma from cobbles of granite and gneiss derived from the Sanandaj–Sirjan belt that were sampled from the Pleistocene Kuh-e-Farangui conglomerates in the High Zagros (Homke *et al*. 2010). However, this appears to be at variance with the petrological data showing that Miocene sedimentary rocks were composed of Mesozoic–Cenozoic carbonate platform rocks, radiolarian cherts, volcanic rocks and ultramafic sources. The relatively lower amount of metamorphic and plutonic clasts from the Sanandaj–Sirjan Zone suggests either a limited contribution, or instead multiple recycling, otherwise metamorphic fragments, plagioclase and K-feldspar as well as quartz would have been much more abundant. To account for this we suggest that the detrital grains cooled in the Sanandaj–Sirjan Zone and High Zagros during the Eocene and the Mesozoic and were deposited in a Palaeocene–Eocene clastic basin, then eroded once more during the Zagros collision.

Late Oligocene–Early Miocene exhumational event: the Zagros collision. The Late Oligocene cooling event at *c*. 25 Ma has been reported from the base of the Chahar–Makan section (Razak Formation). It is consistent with geological observations indicating that uplift, erosion and contraction in the Zagros were under way, and that final suturing occurred in the early Miocene. The collision coincided with a reduction in Africa–Eurasia plate convergence and Red Sea opening at 25 Ma (McQuarrie *et al*. 2003). Detrital AFT ages of 22 Ma (Homke *et al*. 2010), from the NW Zagros Basin, are consistent with detrital zircon and AFT ages that record rapid cooling and sedimentation since 19 Ma in the High Zagros (Gavillot *et al*. 2010). The final suturing of Neotethys at this time is further suggested by an AFT grain-age population of 27 Ma reported from a gneiss sample of the Dorud metamorphic complex of the Sanandaj–Sirjan Zone that complements the AFT detrital ages recovered from the foreland synorogenic sediments (Homke *et al*. 2010). We therefore suggest that the detrital AFT age of 25 Ma recorded by this study marks the onset of cooling of source areas associated with orogenic processes in the Zagros collision. In the next section we more specifically discuss the provenance of these apatite grains.

### *Provenance of Miocene foreland sediments and evolution of palaeodrainage patterns south of the Main Zagros Thrust*

The petrographic assemblage presented in the Chahar–Makan section indicates that the Miocene sediment supply was derived chiefly from an eroding landscape in which the marine sedimentary rocks and ophiolitic material from the Neyriz obducted complex were present. Some accessory minerals such as garnet, amphibole and kyanite indicate the recycling of a metamorphic belt, which is represented by the Mesozoic sheared coloured mélange containing HP rocks and by the HP belt of the Sanandaj–Sirjan Zone exposed around Quri, north of the study area (Fig. 4). Together these data confirm that the region between the southernmost edge of the Sanandaj–Sirjan Zone and the obducted ophiolitic complex was the principal source area for the studied sandstones (Fig. 11).

The low-temperature thermochronometry data are consistent with this interpretation, and the transition from younger (Oligo-Miocene) to older (Mesozoic–Eocene) AFT ages between the Razak Formation (19.7–16.6 Ma) and the above Agha Jari and Bk1 Formations (16.6–13.8 Ma) would therefore reflect localized changes in drainage within this source area. This interpretation is supported by several independent lines of evidence. First, higher $D_{par}$ values in apatite crystals found in the Agha Jari and Bk1 Formations indicate a change in source rock. Second, the bulk-rock composition and the clay mineralogy display a change that coincides with the appearance of dolomite and ankerite, Mg and Fe (to a lesser extent) and enriched minerals that together suggest that, from 18.5 Ma onwards, weathering and erosion involved more Fe–Mg-rich mafic and ultramafic source rocks. Third, petrography shows a progressive change in the source of materials, with more sediment lithic grains in the upper units accompanied by a reduction in volcanic lithic grains.

The exhumed source rocks of the Razak sandstones either could still be exposed in the current landscape or could have been originally deposited or tectonically emplaced then removed by erosion. To examine these options, it is worth noting that (U–Th)/He dating of detrital apatites from the Shalamzar and Dinar Bakhtyari conglomerates (depositional ages *c*. 23–17.1 Ma), 100 km to the NW, in the High Zagros, together with an age–elevation profile in the Lajin thrust indicated a rapid cooling event between 19 and 15 Ma (Gavillot *et al*. 2010); that is, rapid exhumation occurred slightly to

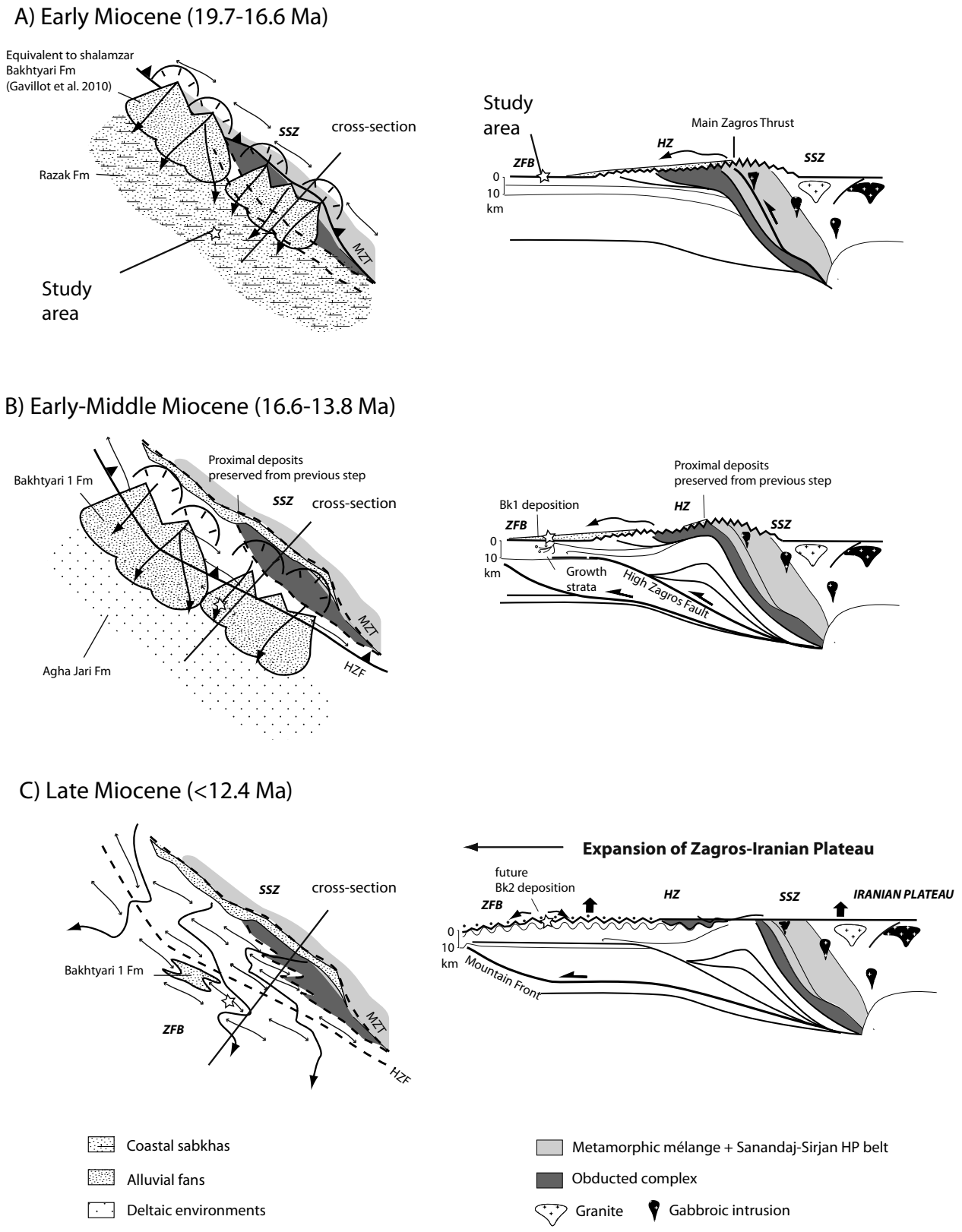


**Fig. 11.** Schematic position of source areas and sedimentation during deformation and uplift of the High Zagros region for (**a**) the early Miocene, (**b**) the early to middle Miocene and (**c**) the late Miocene. The left and right columns show tectonic evolution in cross-section and the type of deposits and the corresponding formations. SSZ, Sanandaj–Sirjan Zone; HZ, High Zagros; ZFB, Zagros Fold Belt; MZT, Main Zagros Thrust; HZF, High Zagros Fault. The southward migration of both the source areas and deformation between stages shown in (**a**) and (**b**) should be noted. Stage (**c**) corresponds to the development of the Zagros folds and expansion of the Zagros and Iranian plateau. At stage (**a**) the Bakhtyari Formation is a lateral equivalent of the Shalamzar Bakhtyari Formation dated to early Miocene (Gavillot *et al*. 2010). The corresponding alluvial deposits record the Miocene exhumation of the Main Zagros Thrust.

the NW of the study area during the early Miocene between the southern Sanandaj–Sirjan Zone and the High Zagros (Fig. 11a). Figure 2 indicates the presence of Neogene conglomerates unconformably overlying the Asmari–Jahrom Formation in the footwall of the Main Zagros Thrust. These Neogene conglomerates are in a structural position similar to the Shalamzar Bakhtyari conglomerates described by Fakhari *et al*. (2008) and Gavillot *et al*. (2010) and are probably correlative and of the same age. This would indicate that the marine sandstones of the Razak Formation in the subsiding foreland were probably connected upstream to these conglomerates (Fig. 11a). If correct, the 25 Ma AFT age documented in the Razak sandstones (Fig. 10) could therefore be interpreted as the record of the exhumation in the hanging wall of the Main Zagros Thrust. The nature of the clasts in the Razak Formation shows that the Neyriz ophiolites were also exposed in the Miocene catchments. As deformation and folding migrated southwards *c*. 14–15 Ma, as attested by growth strata (Khadivi *et al*. 2010), the early Miocene proximal sedimentary rocks located close to the Main Zagros Thrust were uplifted and eroded (Fig. 11b).

Sediment reworking must have occurred and the 25 Ma AFT cooling age should have been observed in the basin section. This is not recorded most probably because the proximal sediment source with the 25 Ma age was significantly eroded in response to folding and outward propagation of the uplifted region of the High Zagros. The resulting rearrangement of the drainage system into axial rivers led to disconnection with upstream catchments. Since then, the fluvial network has remained positioned on slowly eroding catchments characterized by relatively older Mesozoic and Eocene AFT ages corresponding to the Neyriz obducted complex and the southern part of the Sanandaj–Sirjan Zone.

### *Miocene climate and expansion of the Zagros–Iranian plateau*

Clay mineralogy and sedimentology of the synorogenic deposits both emphasize that climate was chiefly warm and dry with no marked changes between 19.7 and 13.8 Ma in the northern Zagros. Very similar sedimentary environments are observed in synorogenic deposits of the southern Alborz foreland basin, indicating a consistently hot and arid climate for the period between 17.5 and 13.8 Ma (Ballato *et al*. 2008). Such aridity is independently confirmed by an increase of the oxygen isotope ratio reported from soil carbonates between *c*. 17.5 and 13.2 Ma possibly linked to the isolation of the Iran region from the incoming moisture of Paratethyan derived air masses (Ballato *et al*. 2010). The presence of palygorskite and the absence of kaolinite, especially above the deltaic deposits of the Razak–Agha Jari transition, record the alteration of carbonaceous soils and sabkhas under arid climate conditions. Overall, the geological evidence for early Miocene aridity is consistent with the marine gypsum deposits reported in the Razak Formation (Mouthereau *et al*. 2007*b*; Khadivi *et al*. 2010). On a broader scale, continental evaporite deposits in the Oligocene Lower Red Formation show that aridity predates the Miocene (e.g. Morley *et al*. 2009). Overall, the recent research in the Iran region, including our results, supports previous studies that considered initiation of aridity in Central Asia (e.g. Kazakhstan) to date back to the late Oligocene, *c*. 24 Ma (Sun *et al*. 2010), which resulted from the Para-Tethys retreat and the Tibetan plateau uplift as suggested by modelling of the Asian climate (e.g. Ramstein *et al*. 1997; Zhang *et al*. 2007).

Marine sedimentation dominated in the study area at least until *c*. 15 Ma (Khadivi *et al*. 2010). We note that this occurred after the deposition of the marine Qom carbonates recording the last marine incursion in Central Iran (e.g. Morley *et al*. 2009, and references therein). From this time onwards, available temporal constraints from surrounding collision belts indicate that shortening and uplift focused in regions bordering the Iranian plateau, including the Zagros, between 15 and 5 Ma (e.g. Mouthereau 2011, and references therein). The widening of the Zagros–Iranian Plateau through the development of new thrusts or folds in the Zagros was probably favoured by the imbalance between the limited erosion under the prevailing arid conditions and tectonics. The development of internally drained areas in the northern Zagros–Iranian Plateau region probably reduced the erosional capacity within channels by disconnecting streams from a stable regional base level (e.g. Sobel *et al*. 2003). This prevented the establishment of a positive feedback between tectonics and erosion and therefore facilitated plateau expansion. Growth strata in the Bakhtyari 1 Formation and the minimum age for the unconformity between Bk1 and Bk2 reveal that deformation propagated into the northern part of the Zagros Fold Belt after 12.4 Ma (Fig. 11b), which is in agreement with Apatite (U–Th)/He (AHe) exhumation ages of 12–8 Ma documented in the southeastern High Zagros across the High Zagros Fault (Gavillot *et al*. 2010). This timing is in agreement with other age constraints on deformation in the Alborz (Guest *et al*. 2007), in the southern Alborz wedge-top basin (Ballato *et al*. 2008), in the Kopet-Dagh (Hollingsworth *et al*. 2010) and in Central Iran (Morley *et al*. 2009). More generally, timing of deformation and shortening estimates throughout the Arabia–Eurasia collision indicate that the regional topography developed through the expansion of the Iranian Plateau towards surrounding collision belts in the Late Miocene–Pliocene, as a result of progressive thickening of the originally thin Iranian continental lithosphere (Morley *et al*. 2009; Mouthereau 2011). This finding, together with the observed stable northward motion of the Arabian plate since the Miocene, does not support a significant role of mantle-scale processes (e.g. slab detachment, delamination) in the building of the regional topography.

## Conclusions

Petrography and AFT thermochronological data presented here show that the Arabia–Eurasia plate boundary has a long history of deformation that extends back into the Mesozoic. Jurassic to Early Cretaceous (174–119 Ma), Palaeocene–Eocene (66–39 Ma) and Late Oligocene (*c*. 25 Ma) AFT grain-age populations are interpreted as cooling events associated with exhumation–magmatism in the southern Sanandaj–Sirjan belt. The timing of change from underplating of the stretched Arabian margin ('soft' collision) to widespread crustal thickening and deformation in the Zagros region, which has been a matter of debate, is constrained here to be no younger than 19.7 Ma. This is indicated by the Mesozoic to Eocene detrital apatite grains originating from the Iranian plate found in the synorogenic foreland sediments of the Agha Jari Formation and more specifically by the AFT ages of 25 Ma observed in the Razak Formation related to cooling in the hanging wall of the Main Zagros Thrust.

Provenance analysis of sedimentary rocks shows that they were derived chiefly from the erosion of marine sedimentary rocks and ophiolitic elements of the Neyriz obducted complex. A component of metamorphic minerals provides further evidence for the recycling of a metamorphic belt and therefore confirms that this portion of the foreland was connected upstream to the southernmost Sanandaj–Sirjan Zone and the obducted ophiolitic complex *c*. 15 Ma.

The transition from younger Late Oligocene to older Mesozoic to Eocene AFT ages between the Razak Formation (19.7–16.6 Ma) and overlying Agha Jari and Bakhtyari Formations (16.6–13.8 Ma) is interpreted to reflect a change in the palaeodrainage distribution as a result of river drainages changing in response to folding and

expansion–uplift of the Zagros–Iranian Plateau region of the High Zagros. This was followed by the removal of the formerly deposited sedimentary rocks to the north containing Late Oligocene AFT ages. Since then, the obducted ophiolites and the southernmost Sanandaj–Sirjan Zone containing older AFT grain-age populations have remained a constant source in the eroding landscape. The clay assemblage shows that these changes have no clear correlation with climate, which was chiefly warm and dry with no marked change throughout the studied time interval. The imbalance between the limited erosion in the Zagros owing to prevailing arid climatic conditions and convergent tectonics permitted the widening of the Zagros–Iranian Plateau region during the Late Miocene.

The authors acknowledge the Geological Survey of Iran for the logistic and administrative support provided during sampling, and especially S. Kargar for his kind help during previous field surveys. This work has been supported by the INSU-Relief programme funded to F. Mouthereau. F. Mouthereau acknowledges contributions by C. Morley and an anonymous reviewer as well as an Advisory Editor and Editor A. Carter for their insightful comments, which greatly improved the overall quality of the paper.

## References


Adatte, T., Stinnesbeck, W. & Keller, G., 1996. Lithostratigraphic and mineralogic correlations of near K/T boundary sediments in northeastern Mexico: implications for origin and nature of deposition. *Geological Society of America, Special Paper*, **307**, 211–226.

Agard, P., Omrani, J., Jolivet, L. & Mouthereau, F. 2005. Convergence history across Zagros (Iran): constraints from collisional and earlier deformation. *International Journal of Earth Sciences*, **94**, 401–419.

Ahmadhadi, F., Lacombe, O. & Daniel, J.-M. 2007. Early reactivation of basement faults in Central Zagros (SW Iran): evidence from pre-folding fracture populations in Asmari Formation and lower Tertiary paleogeography. In: Lacombe, O., Lavé, J., Verges, J. & Roure, F. (eds) *Thrust Belts and Foreland Basins: From Fold Kinematics to Hydrocarbon Systems*. Springer, Berlin, 205–228.

Allen, M.B. & Armstrong, H.A. 2008. Arabia–Eurasia collision and the forcing of mid-Cenozoic global cooling. *Palaeogeography, Palaeoclimatology, Palaeoecology*, **265**, 52–58.

Allen, M., Jackson, J.A. & Walker, R. 2004. Late Cenozoic reorganization of the Arabia–Eurasia collision and the comparison of short-term and long-term deformation rates. *Tectonics*, **23**, TC2008, doi:10.1029/2003TC001530.

Babaie, H.A., Babaei, A., Ghazi, M.A. & Arvin, M. 2006. Geochemical, $^{40}Ar/^{39}Ar$ age, and isotopic data for crustal rocks of the Neyriz ophiolite, Iran. *Canadian Journal of Earth Sciences*, **43**, 57–70.

Ballato, P., Nowaczyk, N.R., Landgraf, A., Strecker, M.R., Friedrich, A. & Tabatabaei, S.H. 2008. Tectonic control on sedimentary facies pattern and sediment accumulation rates in the Miocene foreland basin of the southern Alborz mountains, northern Iran. *Tectonics*, **27**, TC6001, doi:10.1029/2008TC002278.

Ballato, P., Mulch, A., Landgraf, A., Strecker, M.R., Dalconi, M.C., Friedrich, A. & Tabatabaei, S.H. 2010. Middle to late Miocene Middle Eastern climate from stable oxygen and carbon isotope data, southern Alborz mountains, N Iran. *Earth and Planetary Science Letters*, **300**, 125–138, doi:10.1016/j.epsl.2010.09.043.

Ballato, P., Uba, C.E. *et al.* 2011. Arabia–Eurasia continental collision: insights from late Tertiary foreland–basin evolution in the Alborz Mountains, northern Iran. *Geological Society of America Bulletin*, **123**, 106–131, doi:10.1130/B30091.1.

Berberian, F. & Berberian, M. 1981. Tectono-plutonic episodes in Iran. *In:* Gupta, H.K. & Delany, F.M. (eds) *Zagros–Hindu Kush–Himalaya Geodynamic Evolution*. American Geophysical Union, Geodynamics Series, **3**, 5–32.

Berberian, M. & King, G.C.P. 1981. Towards a paleogeography and tectonic evolution of Iran. *Canadian Journal of Earth Sciences*, **18**, 210–265.

Berberian, F., Muir, I.D., Pankhurst, R.J. & Berberian, M. 1982. Late Cretaceous and early Miocene Andean-type plutonic activity in northern Makran and Central Iran. *Journal of the Geological Society, London*, **139**, 605–614.

Chamley, H. 1989. *Clay Sedimentology*. Springer, Berlin.

Chamley, H., Deconinck, J.F. & Millot, G. 1990. Sur l'abondance des minéraux smectitiques dans les sédiments marins communs déposés lors des périodes de haut niveau marin du Jurassique au Paleogene. *Comptes Rendus de l'Académie des Sciences*, **311**, 1529–1536.

Deconinck, J.F. & Chamley, H. 1995. Diversity of smectite origins in Late Cretaceous sediments: example of chalks from northern France. *Clay Minerals*, **30**, 365–379.

Dickinson, W.R. 1970. Interpreting detrital modes of graywacke and arkose. *Journal of Sedimentary Petrology*, **40**, 695–707.

Fakhari, M.D., Axen, G.J., Horton, B.K., Hassanzadeh, J. & Amini, A. 2008. Revised age of proximal deposits in the Zagros foreland basin and implications for Cenozoic evolution of the High Zagros. *Tectonophysics*, **451**, 170–185.

Galbraith, R.F. & Green, P.F. 1990. Estimating the component ages in a finite mixture. *Nuclear Tracks and Radiation Measurements*, **17**, 197–206.

Galbraith, R.F. & Laslett, G.M. 1993. Statistical models for mixed fission track ages. *International Journal of Radiation Applications and Instrumentation. Part D*, **21**, 459–470.

Gavillot, Y., Axen, G.J., Stockli, D.F., Horton, B.K. & Fakhari, M.D. 2010. Timing of thrust activity in the High Zagros fold–thrust belt, Iran, from (U–Th)/He thermochronometry. *Tectonics*, **29**, TC4025, doi:10.1029/2009TC002484.

Golonka, J. 2004. Plate tectonic evolution of the southern margin of Eurasia in the Mesozoic and Cenozoic. *Tectonophysics*, **381**, 235–273.

Guest, B., Horton, B.K., Axen, G.J., Hassanzadeh, J. & McIntosh, W.C. 2007. Middle to late Cenozoic basin evolution in the western Alborz Mountains: implications for the onset of collisional deformation in northern Iran. *Tectonics*, **26**, TC6011, doi:10.1029/2006TC002091.

Hallam, A. 1976. Geology and plate tectonics interpretation of the sediments of the Mesozoic radiolarite–ophiolite complex in the Neyriz region, southern Iran. *Geological Society of America Bulletin*, **87**, 47–52.

Harzhauser, M., Kroh, A., Mandic, O., Piller, E.W., Gohlich, U., Reuter, M. & Berning, B. 2007. Biogeographic responses to geodynamics: a key study all around the Oligo-Miocene Tethyan Seaway. *Zoologischer Anzeiger*, **246**, 241–256.

Hatzfeld, D. & Molnar, P. 2010. Comparisons of the kinematics and deep structures of the Zagros and Himalaya and of the Iranian and Tibetan plateaus and geodynamic implications. *Review of Geophysics*, **48**, RG2005, doi:10.1029/2009RG000304.

Haynes, S.J. & Reynolds, P.H. 1980. Early development of Tethys and Jurassic ophiolite displacement. *Nature*, **283**, 561–563.

Hempton, M.R. 1987. Constraints on Arabian Plate motion and extensional history of the Red Sea. *Tectonics*, **6**, 687–705.

Hollingsworth, J., Fattahi, M. *et al.* 2010. Oroclinal bending, distributed thrust and strike-slip faulting, and the accommodation of Arabia–Eurasia convergence in NE Iran since the Oligocene. *Geophysical Journal International*, **181**, 1214–1246.

Homke, S., Vergés, J. *et al.* 2009. Late Cretaceous–Paleocene formation of the proto-Zagros foreland basin, Lurestan Province, SW Iran. *Geological Society of America Bulletin*, **121**, 963–978.

Homke, S., Vergés, J. *et al.* 2010. Insights in the exhumation history of the NW Zagros from bedrock and detrital apatite fission-track analysis: evidence for a long-lived orogeny. *Basin Research*, **22**, 659–680.

Houshmand Zadeh, A., Ohanian, A.T. *et al.* 1990. *Geological Map of Eqlid. Quadrangle G10, scale 1:250,000*. Geological Survey of Iran, Tehran.

Ingersoll, R.V., Bullard, T.F., Ford, R.L., Grimm, J.P., Pickle, J.D. & Sares, S.W. 1984. The effect of grain size on detrital modes: a test of the Gazzi–Dickinson point-counting method. *Journal of Sedimentary Petrology*, **54**, 103–116.

James, G.A. & Wynd, J.G. 1965. Stratigraphic nomenclature of Iranian Oil Consortium Agreement Area. *AAPG Bulletin*, **49**, 2162–2245.

Khadivi, S., Mouthereau, F. *et al.* 2010. Magnetochronology of synorogenic Miocene foreland sediments in the Fars arc of the Zagros Folded Belt (SW Iran). *Basin Research*, **22**, 918–932.

Kocsis, L., Vennemann, T.W., Hegner, E., Fontignie, D. & Tütken, T. 2009. Constraints on Miocene oceanography and climate in the Western and Central Paratethys: O-, Sr-, and Nd-isotope compositions of marine fish and mammal remains. *Palaeogeography, Palaeoclimatology, Palaeoecology*, **271**, 117–129.

Kübler, B., 1983. *Dosage quantitatif des minéraux majeurs des roches sédimentaires par diffraction X.* Cahier de l'Institut de Géologie de Neuchâtel, Série AX **1.1–1.2.**

Kübler, B., 1987. *Cristallinité de l'illite, methodes normalisées de preparations, méthodes normalisées de mesures*. Cahiers de l'institut de Géologie de Neuchâtel, Switzerland, Série ADX **1.3**.

Lacombe, O., Mouthereau, F., Kargar, S. & Meyer, B. 2006. Late Cenozoic and modern stress fields in the western Fars (Iran): implications for the tectonic and kinematic evolution of central Zagros. *Tectonics*, **25**, TC1003, doi:10.1029/2005TC001831.

Lacombe, O., Amrouch, K., Mouthereau, F. & Dissez, L. 2007. Calcite twinning constraints on late Neogene stress patterns and deformation mechanisms in the active Zagros collision belt. *Geology*, **35**, 263–266.

Lanphere, M.A. & Pamic, T. 1983. $^{40}Ar/^{39}Ar$ ages and tectonic setting of ophiolites from Neyriz area, south-east Zagros range, Iran. *Tectonophysics*, **96**, 245–256.

Leterrier, J. 1985. Mineralogical, geochemical and isotopic evolution of two Miocene mafic intrusions from the Zagros (Iran). *Lithos*, **18**, 311–329.

Maggi, A. & Priestley, K. 2005. Surface waveform tomography of the Turkish–Iranian Plateau. *Geophysical Journal International*, **160**, 1068–1080.

Masson, F., Anvari, M. *et al.* 2007. Large-scale velocity field and strain tensor in Iran inferred from GPS measurements: new insight for the present-day deformation pattern within NE Iran. *Geophysical Journal International*, **170**, 436–440.

Mazhari, S.A., Bea, F. *et al.* 2009. The Eocene bimodal Piranshahr massif of the Sanandaj–Sirjan Zone, NW Iran: a marker of the end of the collision in the Zagros orogen. *Journal of the Geological Society, London*, **166**, 53–69.

McClusky, S., Reilinger, R., Mahmoud, S., Ben Sari, D. & Tealeb, A. 2003. GPS constraints on Africa (Nubia) and Arabia plate motions. *Geophysical Journal International*, **155**, 126–138.

McQuarrie, N., Stock, J.M., Verdel, C. & Wernicke, B.P. 2003. Cenozoic evolution of Neotethys and implications for the causes of plate motions. *Geophysical Research Letters*, **30**, doi:10.1029/2003GL017992.

Morley, C.K., Kongwung, B. *et al.* 2009. Structural development of a major late Cenozoic basin and transpressional belt in central Iran: the Central Basin in the Qom–Saveh area. *Geosphere*, **5**, 325–362.

Motiei, H. 1993. *Geology of Iran*: *Stratigraphy of Zagros*. Geological Survey of Iran, Tehran.

Mouthereau, F. 2011. Timing of uplift in the Zagros belt/Iranian plateau and accommodation of late Cenozoic Arabia/Eurasia convergence. *Geological Magazine*, **148**, 726–738, doi:10.1017/S0016756811000306.

Mouthereau, F., Lacombe, O. & Meyer, B. 2006. The Zagros Folded Belt (Fars, Iran): constraints from topography and critical wedge modelling. *Geophysical Journal International*, **165**, 336–356.

Mouthereau, F., Lacombe, O., Tensi, J., Bellahsen, N., Kargar, S. & Amrouch, K. 2007*a*. Mechanical constraints on the development of the Zagros Folded Belt (Fars). In: Lacombe, O., Lavé, J., Roure, F. & Verges, J. (eds) *Thrust Belts and Foreland Basins: From Fold Kinematics to Hydrocarbon Systems*. Springer, Berlin, 245–264.

Mouthereau, F., Tensi, J., Bellahsen, N., Lacombe, O., De Boisgrollier, T. & Kargar, S. 2007*b*. Tertiary sequence of deformation in a thin-skinned/thick-skinned collision belt: the Zagros Folded Belt (Fars, Iran). *Tectonics*, **26**, TC5006, doi:10.1029/2007TC002098.

Nilforoushan, F., Masson, F. *et al.* 2003. GPS network monitors the Arabia–Eurasia collision deformation in Iran. *Journal of Geodesy*, **77**, 411–422.

NIOC, 1979. *Geological Map of Shiraz. Quadrangle G11, scale 1:250,000*. National Iranian Oil Company, Tehran.

Okay, A.I., Zattin, M. & Cavazza, W. 2010. Apatite fission-track data for the Miocene Arabia–Eurasia collision. *Geology*, **38**, 35–38.

Paul, A., Hatzfeld, D., Kaviani, A., Tatar, M. & Pequegnat, C. 2010. Seismic imaging of the lithospheric structure of the Zagros mountain belt (Iran). *In*: Leturmy, P. & Robin, C. (eds) *Tectonic and Stratigraphic Evolution of the Zagros and Makran during the Meso-Cenozoic*. Geological Society, London, Special Publications, **330**, 5–18, doi: 10.1144/SP330.2.

Rachidnejad-Omran, N., Emami, M.H., Sabzehei, M., Rastad, E., Bellon, H. & Piqué, A. 2002. Lithostratigraphie et histoire paléozoïque à paléocène des complexes métamorphiques de la région de Muteh, zone de Sanandaj–Sirjan (Iran méridional). *Comptes Rendus de l'Académie des Sciences*, **334**, 1185–1191.

Ramstein, G., Fluteau, F., Besse, J. & Joussaume, S. 1997. Effect of orogeny, plate motion and land–sea distribution on Eurasian climate change over the past 30 million years. *Nature*, **386**, 788–795.

Reuter, M., Piller, W.E. *et al.* 2009. The Oligo-Miocene Qom Formation (Iran): evidence for an early Burdigalian restriction of the Tethyan Seaway and closure of its Iranian gateways. *International Journal of Earth Sciences*, **98**, 627–650.

Ricou, L.E. 1976. Evolution structurale de Zagrides. La region clef de Neyriz (Zagros iranien). Memoires de la Société Géologique de France, **126**.

Robert, C. & Chamley, H. 1990. Paleoenvironmental significance of clay mineral association at the Cretaceous–Tertiary boundary. *Palaeogeography, Palaeoclimatology, Palaeoecology*, **79**, 205–219.

Robin, C., Gorican, S., Guillocheau, F., Razin, P., Dromart, G. & Mosaffa, H. 2010. Mesozoic deep-water carbonate deposits from the southern Tethyan passive margin in Iran (Pichakun nappes, Neyriz area): biostratigraphy, facies sedimentology and sequence stratigraphy. In: Leturmy, P. & Robin, C. (eds) *Tectonic and Stratigraphic Evolution of Zagros and Makran During the Mesozoic–Cenozoic*. Geological Society, London, Special Publications, **330**, 179–210.

Sarkarinejad, K. & Alizadeh, A. 2009. Dynamic model for the exhumation of the Tutak gneiss dome within a bivergent wedge in the Zagros Thrust System of Iran. *Journal of Geodynamics*, **47**, 201–209.

Sarkarinejad, K. & Azizi, A. 2008. Slip partitioning and inclined dextral transpression along the Zagros Thrust System, Iran. *Journal of Structural Geology*, **30**, 116–136.

Sarkarinejad, K., Godin, L. & Faghih, A. 2009. Kinematic vorticity flow analysis and $^{40}Ar/^{39}Ar$ geochronology related to inclined extrusion of the HP–LT metamorphic rocks along the Zagros accretionary prism, Iran. *Journal of Structural Geology*, **1**, 691–706.

Schuster, F. & Wielandt, U. 1999. Oligocene and Early Miocene coral faunas from Iran: palaeoecology and palaeobiogeography. *International Journal of Earth Sciences*, **88**, 571–581.

Sheikholeslami, M.R., Pique, A., Mobayen, P., Sabzehei, M., Bellon, H. & Hashem Emami, M. 2008. Tectono-metamorphic evolution of the Neyriz metamorphic complex, Quri-Kor-e-Sefid area (Sanandaj–Sirjan Zone, SW Iran). *Journal of Asian Earth Sciences*, **31**, 504–521.

Sobel, E.R., Hilley, G.E. & Stecker, M.R. 2003. Formation of internally drained contractional basins by aridity-limited bedrock incision. *Journal of Geophysical Research*, **108**, 2344, doi:10.1029/2002JB001883.

Stocklin, J. 1968. Structural history and tectonics of Iran: a review. *AAPG Bulletin*, **52**, 1229–1258.

Sun, J., Ye, J. *et al.* 2010. Late Oligocene–Miocene mid-latitude aridification and wind patterns in the Asian interior. *Geology*, **38**, 515–518.

Tatar, M., Hatzfeld, D., Martinod, J., Walperdorf, A., Ghafori-Ashtiany, M. & Chéry, J. 2002. The present-day deformation of the central Zagros from GPS measurements. *Geophysical Research Letters*, **29**, doi:10.1029/2002GL015427.

Verdel, C., Wernicke, B.P., Ramezani, J., Hassanzadeh, J., Renne, P.R. & Spell, T.L. 2007. Geology and thermochronology of Tertiary Cordilleran-style metamorphic core complexes in the Saghand region of central Iran. *Geological Society of America Bulletin*, **119**, 961–977.

Verdel, C., Wernicke, B.P., Hassanzadeh, J. & Guest, B. 2011. A Paleogene extensional arc flare-up in Iran. *Tectonics,* **30**, TC3008, doi: 10.1029/2010tc002809.

Vernant, P., Nilforoushan, F. *et al.* 2004. Present-day crustal deformation and plate kinematics in the Middle East constrained by GPS measurements in Iran and northern Oman. *Geophysical Journal International*, **157**, 381–398.

Vincent, S.J., Allen, M.B., Ismail-Zadeh, A.D., Flecker, R., Foland, K.A. & Simmons, M.D. 2005. Insights from the Talysh of Azerbaijan into the Paleogene evolution of the South Caspian region. *Geological Society of America Bulletin*, **117**, 1513–1533.

Weaver, C.E. 1989. *Clays, Muds and Shales*. Elsevier, Amsterdam.

Yamato, P., Kaus, B.J.P., Mouthereau, F. & Castelltort, S. 2011. Dynamic constraints on the crustal-scale rheology of the Zagros fold belt, Iran. *Geology*, **39**, 815–818, doi:10.1130/G32136.1.

Zhang, Z., Wang, H., Guo, Z. & Jiang, D. 2007. What triggers the transition of palaeoenvironmental patterns in China, the Tibetan Plateau uplift or the Paratethys Sea retreat? *Palaeogeography, Palaeoclimatology, Palaeoecology*, **245**, 317–331.

Received 8 March 2011; revised typescript accepted 18 July 2011.
Scientific editing by Andrew Carter.